Biophysical Methods and Data Analysis for Simulating Overland Flow in the Everglades

by Judson W. Harvey and Jay Choi

U.S. Geological Survey, Earth System Processes Division, Reston, VA

colleague reviewed and U.S. Geological Survey Bureau approved, May 9, 2022

Contents

A. Abstract

The Everglades in south Florida supply fresh drinking water for more than 7 million people, host a National Park, and are classified as a Ramsar wetland of international distinction. Predicting trajectories of water flow and water storage changes in the future is important to managing the Congressionally authorized restoration of the Everglades. Here we describe the needed data sources and analysis approaches to build the inputs for biophysically based modeling that can protect water and ecological resources in the face of changing water management and climate conditions.

A biophysical approach to modeling overland flow in the Everglades can help predict future outcomes for ecological habitat, water storage during droughts, and water conveyance during floods. The needed data include measurements of vegetation stem architecture, microtopography, and landscape pattern metrics. Stem architecture measurements present the opportunity to estimate flow roughness of distinct vegetation communities based on hydraulic principles. At a larger scale, the microtopography and the connectivity of the sloughs between ridges offer a way to quantify the effects of flow blockage and tortuous flow paths on overland flow. Combined with theory these data provide the capacity to simulate overland flow in both the historical, pre-drainage Everglades as well as in the present-day managed Everglades. Also provided are the hydrologic data, e.g., water slopes, water depths and overland flow velocities, that can be used to verify a biophysical model. Ultimately, the purpose is to anticipate how changing flow and water depth will interact with evolving vegetation and landscape conditions to influence future water availability for society and for the ecosystem, both in the Everglades and in other low-gradient floodplains.

B. Overview of the associated data release

This report describes data sources and analysis approaches for biophysical data supporting simulations of overland flow in the Everglades. The accompanying data release (https://doi:10.5066/P9DQYB1O) includes six types of information:

(1) vegetation architecture and calculated roughness as it varies with height above the ground surface analyzed from previously published field measurements of vegetation stem frontal area and stem diameter at approximately 60 locations in the Everglades. See data release file **USGS_20HWCOLL0003_Vegetation Architecture and Roughness.xlsx**

(2) microtopography summaries of previously published field measurements of the variability in ground surface elevation within 57 primary sampling units (PSUs). See data release file **USGS_20HWCOLL0003_Microtopography.xlsx**

(3) 23 binarized ridge-slough vegetation maps based on previously published vegetation maps from 20 PSUs. See data release file **USGS_20HWCOLL0003_R-S Binary Landscape Data.zip**

(4) landscape metrics that summarize the spatial arrangement of ridges and sloughs based on analysis of ridge aerial proportion, slough directional connectivity, ridge anisotropy, and ridge-slough edge fractal dimension within 23 circular areas (approximately 2-km^2) that were sub-setted for analysis from the 20 binarized ridge-slough vegetation maps. See data release file **USGS_20HWCOLL0003_Landscape metrics.xls**

(5) input parameters and outputs of overland flow simulations. See data release file **USGS_20HWCOLL0003_Inputs and Outputs_All Simulation Cases.xls**.

(6) Hydrologic data to compare with biophysical simulations of present-day overland flow, including published observations of water depth, slope, flow velocity, and discharge measured at 5 locations in four sub-basins of the Everglades for comparison with BioFRE. See data release file **USGS_20HWCOLL0003_Hydrologic data for validation.xls**.

C. Data sources

To analyze biophysical controls on overland flow we needed vegetation community data and stem architecture data, as well as ground elevation data, which were acquired from publications by scientists from the U.S. Geological Survey (USGS) Greater Everglades Priority Ecosystem Studies (GEPES) program (Harvey et al., 2009, 2011, 2005; Carter et al., 1999a, 1999b; and Rybicki et al., 2001, 2002) and publications by scientists from the RECOVER program of the Army Corps of Engineers (Ross et al., 2015). Here we briefly summarize methods of data collection as an aid in understand our analysis approaches.

We analyzed data sources and averaged results across several scales of observations, including approximately sixty locations where vegetation stem architecture was measured (Figure 1), and fifty-seven, 2 x 5 km primary sampling units (PSUs) where microtopography was measured and vegetation communities mapped (Figures 2 and 3). Nine Everglades sub-basins were established for data analysis, as shown in Figures 2 and 3. The sub-basins were delineated by grouping nearby PSUs in areas that experience a similar degree of hydrologic isolation between levees, or because of similarity in the duration and depth of surface water inundation, i.e., hydroperiod. Hydroperiod varies along north-south and east-west gradients because of proximity to surface water inflows, gradients in land surface elevation, peat subsidence history,

gradients in peat depth, aquifer transmissivity, and water use outside the Everglades that may cause drying in the Everglades (McVoy et al., 2011; Harvey et al. 2017).

C-1. Field measurements of vegetation architecture

Sampling of stem architecture of Everglades vegetation began in 1999 with the purpose to estimate drag forces and effects on flow and water depth. Researchers measured stem frontal area and stem diameter on vegetation samples from 0.25 m^2 plots that were harvested from approximately sixty locations across the Everglades (Harvey et al., 2009, 2011, 2005; Carter et al., 1999a, 1999b; and Rybicki et al., 2001, 2002). For this application we use the data acquired from Everglades National Park, WCA-3A, and WCA-2A between 1999 and 2005 (Harvey et al., 2009, 2005; Carter et al., 1999a, 1999b; and Rybicki et al., 2001, 2002) that were compiled by Larsen et al. (2009) (Figure 4). The relevant metrics of vegetation architecture include the stem frontal area, a [1/cm], and the stem diameter, d [cm], which were measured using the methods described by Harvey et al. (2009, 2011, 2005).

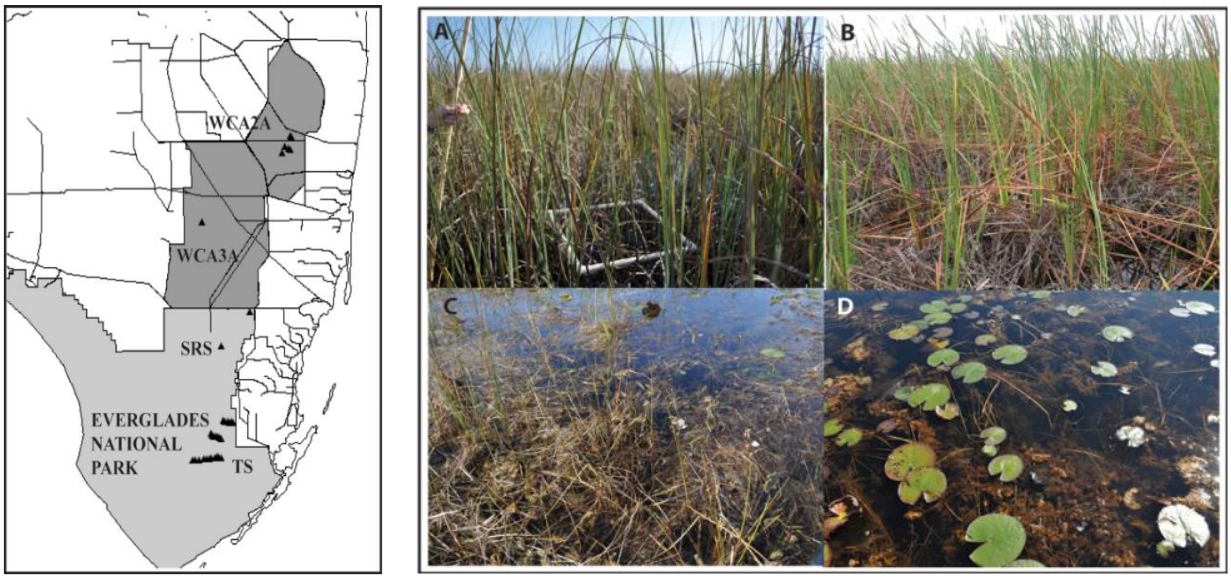

Figure 1. Vegetation sampling locations (left panel) and photographs of four major community types, Sawgrass ridge community (A), Cattail community (B), Spikerush slough community (C), and Deepwater Slough with Water Lily community. Cattail community data were not used in the present study. Photographs by the U.S. Geological Survey

For this study we used measurements of stem architecture characterizing four vegetation community types: (1) Sawgrass ridge community vegetated primarily with Sawgrass (*Cladium jamaicense*), (2) Spikerush slough community vegetated primarily with Spikerush (*Eleocharis* spp.), (3) Deepwater Sough community vegetated primarily with Water Lily (*Nuphar odorata*), and (4) Spikerush slough community vegetated with a mixture of Spikerush and Bladderwort (*Utricularia purpurea*), which grows as a floating mat covered with thick coatings of attached periphyton.

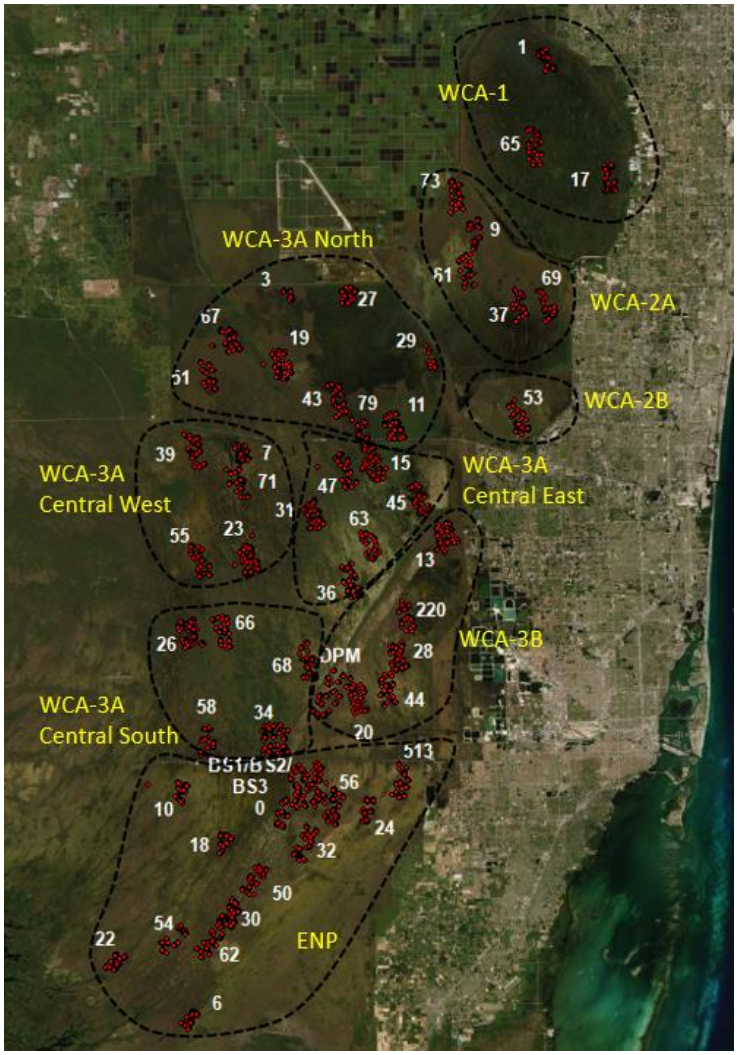

Figure 2. Areas of Everglades microtopography measurement and local vegetation classification are shown in red and labeled in white with the corresponding PSU (primary sampling unit) number. Black dashes delineate sub-basins labeled in yellow for which data were summarized for this study. The original data were provided by Ross et al. (2015) and results of additional data processing are explained in the text. Base imagery acquired from ESRI, ArcGIS, ArcMap 10.8.1.

C-2. Microtopography measurements and ground-based vegetation classification

Between 2010 to 2015, researchers under contract to the Army Corps of Engineers on the project known as RECOVER collected ground-based measurements of microtopography and noted nearby vegetation type (Ross et al, 2015). Because of the importance of the RECOVER data sets to our present work, we briefly recount the field sampling and mapping methods. We refer to Ross et al. (2015) and Ross et al. (2003) for the definitive information about RECOVER data collection and treatment.

The field sampling was undertaken in designated 2 x 5 km PSUs (Figure 2) that were accessed by airboat or helicopter when water levels were moderate but high enough to access all randomly selected areas within a PSU. To randomize sampling locations, each PSU was

subdivided in 80 equal area zones (250 m x 500 m) in which a sampling cluster point was randomly located, at which the center of the cluster was sampled as well as two additional sampling sites that were randomly selected for distance and direction away from the cluster center point. At all sampling locations water depths were measured that could be analyzed to describe microtopographic variation. Water depth was measured using a standard measuring tool with a standard amount of pressure applied to measure the depth from the water surface to top of the peat. All totaled, water depth measurements were made at 8568 locations.

Ross et al. (2015) estimated ground surface elevations from the measured water depths by converting water depths to ground elevations using the Everglades Depth Estimation Network (EDEN) tool (Jones et al., 2012). EDEN was used to reference the locally measured water depth with EDEN's model estimated water surface elevation for the same day. The absolute elevation of the ground surface at the location of the water depth measurement was computed as:

$$Abs\_Elev_{point} = WSE_{EDEN} - Water\ depth_{point} \qquad Eq.\ 1$$

where,

Abs_Elev_{point} = absolute ground surface elevation

WSE_{EDEN} = EDEN model estimated local water surface elevation on the date of measurement

$\text{Water depth}_{point}$ = measured water depth

Accompanying each depth measurement was a ground-based assessment of vegetation type within a 25-m radius of the depth measurement. See Ross et al. (2015) for additional details about ground elevations and ground-based vegetation assessments.

C-3. Vegetation maps

Vegetation mapping was performed by RECOVER scientists (Ross et al., 2015) using techniques of aerial photogrammetry. Researchers used base imagery consisting of either color infrared CERP aerial imagery acquired by CERP (Central Everglades Restoration Project) uses images collected in 2003 or 2009 for PSUs 4 and 5 and PSUs 0 and 14, respectively, or National Agriculture Imagery Program (NAIP) 2010 color infrared aerial imagery for the other 44 PSUs and the DPM area. The observed indicators of vegetation community within each PSU were mapped according to the classification system developed by a consortium of south Florida vegetation scientists following Rutchey et al. (2006). A minimum mapping resolution of 200 m^2 was achieved for non-woody vegetation and 36 m^2 for tree islands. The area mapped within each PSU varied by year with mapping of the full 2 km x 5 km extent of PSUs in the first year compared to the 2nd year when a central 2 km x 2 km portion within each PSU was mapped. See Ross et al. (2015) for additional details about vegetation mapping.

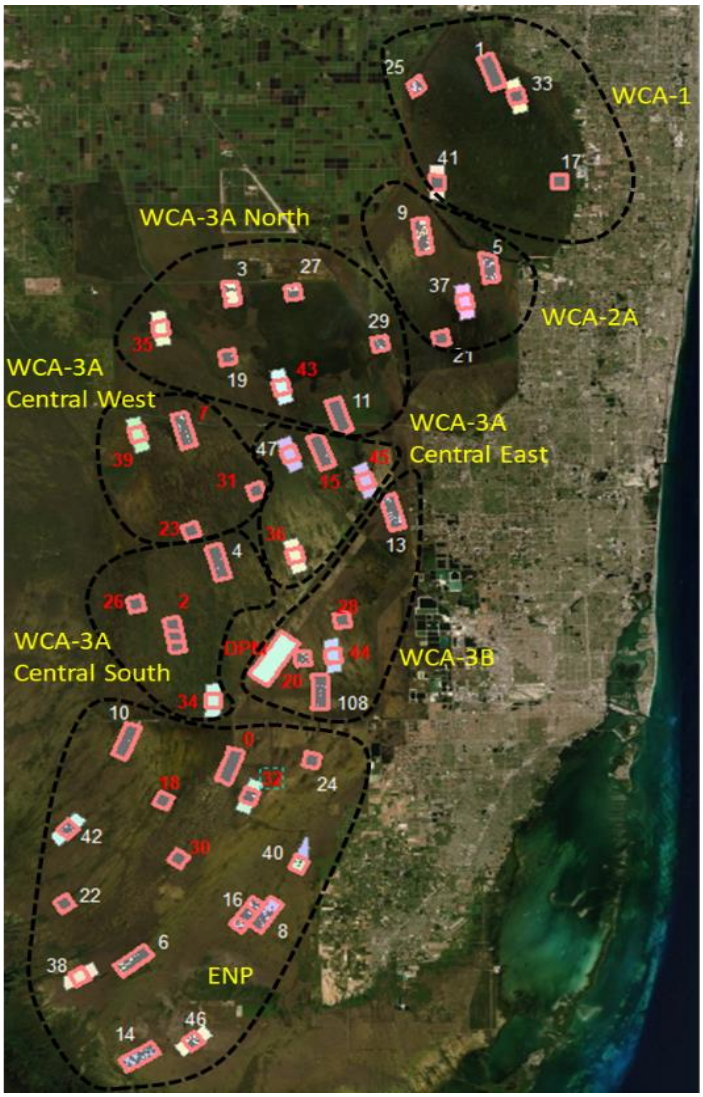

Figure 3. Forty-nine mapped areas of Everglades vegetation (pink boundaries) identified by their overlap with numbered PSUs (2 x 5 km PSUs shown in white). From among 49 vegetation maps we selected 20 PSUs (numbered in red) for detailed analysis of landscape pattern. Original vegetation maps from Ross et al. (2015) were further analyzed to quantify landscape pattern as explained in the text. Black dashed lines and yellow lettering designate sub-basins for summarizing landscape pattern metrics. Base imagery acquired from ESRI, ArcGIS, ArcMap 10.8.1.

D. Data preparation

The data sources characterize vegetation architecture, microtopography, and landscape pattern at dozens of sites across the central Everglades. Hydrologic modeling rarely uses individual point data and more typically uses averaged data that represent conditions over larger areas. In this section we describe the analysis approaches as well as averaging approaches across relevant areas including 2 x 5 km PSUs and larger scale sub-basins in the Everglades. We also describe analysis approaches to prepare model inputs.

D-1. Vegetation architecture data preparation for roughness calculations

Biophysical estimates of roughness are based on two measures of vegetation architecture, stem vegetation frontal area, a [L^{-1}] and average stem diameter, d, [L]. Roughness calculations were made for five vegetation communities: a) Sawgrass ridge (*C. jamaicense*), b) Spikerush slough (*Eleocharis* spp.), c) Sparse Spikerush slough, d) Deep-water slough (Water Lily, e.g., *Nuphar odorata*), and e) Spikerush slough plus the floating aquatic Bladderwort (*Utricularia purpurea*) with periphyton attached. Mean values of stem architecture were used as shown in Figure 4 except for Sparse Spikerush slough, where the mean plus 20% of the range for frontal area and the mean minus 20% of the range for stem diameter were used (Figure 4).

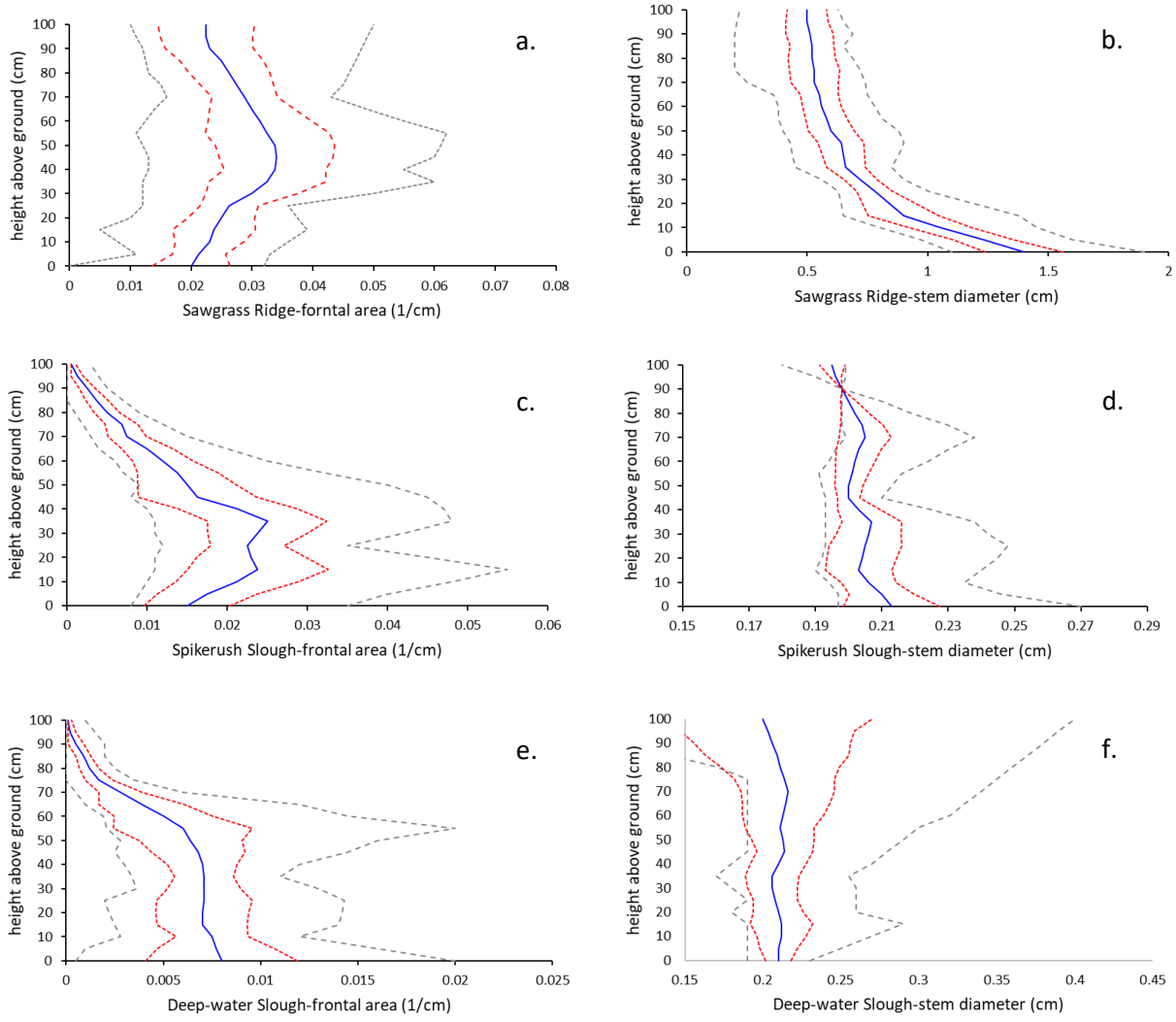

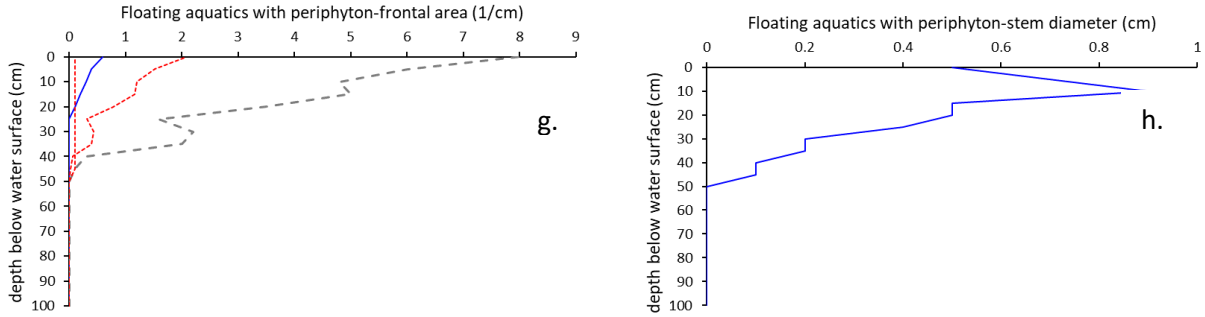

Figure 4. Everglades vegetation frontal area and stem diameter versus height above the ground surface for Sawgrass ridge (panels a and b), Spikerush slough (panels c and d), Deepwater slough (panels e and f), and floating aquatics and periphyton (panels g and h). Blue lines are mean values, red lines are mean +/- 20% of the range, and dashed grey lines are the minimum and maximum values.

The theory and approach to calculating a biophysical roughness coefficient are explained in detail ahead. The purpose was to build a crosswalk between hydraulic theory of flow through vegetation and the more commonly used empirical expression for modeling overland flow. The result is a roughness coefficient for use in overland flow modeling that is transferable to other sites and other water depths rather than being calibrated based on fitting to hydrologic data collected at specific sites and water depths.

Here the approach is summarized. A biophysically based roughness coefficient was calculated by equating the biophysically based expression for velocity, eq. [4], with an empirical expression for velocity known as Manning's equation, eq. [5]. The expanded equation was rearranged to solve for the biophysically based roughness coefficient. The biophysical parameters include the incremental depth-averaged values of frontal area and stem diameter from Figure 4 as well as vegetation-specific drag coefficients (Table 1) and a water slope estimate, *S*, for which a typical slope of 2E10-5 was used to standardize calculations. The result was depth-averaged calculations of roughness for four vegetation communities that vary in 10-cm increments of water depth between 10 and 100 cm.

D-2. Drag theory method to calculate roughness

Here we explain how to combine measurements of stem architecture with hydraulic theory to compute stem-architecture and depth-dependent roughness coefficients that vary between vegetation community. Roughness estimation was based in physically based modeling of flow resistance in wetlands that specifies how the stem frontal area and stem diameter influence drag and flow velocity for a given water slope, i.e., the driving force for flow. The drag expression is defined as a part of the overall force balance:

$$gS = \frac{1}{2} C_d a U^2 \qquad Eq. 2$$

where U is depth-averaged velocity (LT^{-1}), g is gravity (LT^{-2}), S is water surface slope ($L\ L^{-1}$), a is depth-averaged frontal area of vegetation stems per unit volume (L^{-1}), and C_d is the bulk drag coefficient on vegetation. Following Nepf (1999) and Harvey et al. (2009), the drag coefficient for flow through emergent vegetation is:

$$C_d = 2K_0 {R_e}^{-k} (ad)^{-0.5} \qquad Eq. 3$$

where average stem diameter, d (L), is the second variable describing vegetations architecture, accompanying the stem frontal area, a. The drag expression accounts for the dependence of drag on flow conditions. Specifically, for conditions of laminar flow, the drag is a negative function of Reynolds number as described by the constants K_o and k, which indicate the slope and intercept of a negative relation between drag and the stem Reynolds number, $Re_d = {Ud}/{v}$, where v is the kinematic viscosity (L^2/T) (Harvey et al., 2009). We were fortunate to have the previously published stem architecture measurements and the empirical constants describing the dependency of drag on flow condition (Harvey et al., 2009; Larsen et al., 2009).

Harvey et al. (2009) substituted equation [3] into [2] and rearranged the result to develop a biophysical flow rate expression that simulates flow through a single vegetation community with the following expressions for unit-width discharge and flow velocity:

$$q = h\left\{\frac{gS\boldsymbol{d}^{2.5-\varphi}}{K_0 v^{2-\varphi}\boldsymbol{a}^{0.5}}\right\}^{1/\varphi} \quad and \quad U = \left\{\frac{gS\boldsymbol{d}^{2.5-\varphi}}{K_0 v^{2-\varphi}\boldsymbol{a}^{0.5}}\right\}^{1/\varphi} \qquad Eq. 4$$

where variables are previously defined except for φ which equals 2 - k and which helps simplify.

In order to calculate roughness from biophysical variables, the biophysically based flow rate expression for velocity given in eq. [4] was set equal to the following version of Manning's rate law:

$$U = \frac{1}{n} h^{\frac{2}{3}} S^1 \qquad Eq.\ 5$$

where n is a roughness coefficient known as Manning's "n"[$T/L^{1/3}$]; h= water depth [L]; and other variables are previously defined. Rearranging the expanded equation yields*:*

$$n_b = \frac{h^{2/3} S^1}{\left\{\frac{gS\boldsymbol{d}^{2.5-\varphi}}{K_0 v^{2-\varphi}\boldsymbol{a}^{0.5}}\right\}^{1/\varphi}} \qquad Eq.\ 6$$

which provides a biophysically based estimate of the roughness coefficient, n_b, where subscript b (for biophysical) will usually be replaced with a subscript describing roughness computed for a vegetation community such as the roughness for for the slough, n_s, or the ridge, n_r.

In the laminar flow range the vegetation roughness scales with flow velocity as affected by the transition between creeping flow around stems to emergence and shedding or vortices behind stems at higher Reynolds number. The analysis of flow roughness is therefore complicated in the laminar flow range because flow drag decreases as velocity increases until the onset of turbulence where roughness becomes relatively constant (Harvey et al., 2009). The dependency of drag in the laminar flow range is accounted for in eq. [6] by the vegetation specific drag coefficients (K_0 and k) for ridge and slough vegetation communities. Those coefficients and the drag coefficient ζ for floating aquatics, are provided in Table 1. A caution is issued however because eq. [5] does not identify a turbulent threshold to signal when roughness becomes a constant. Using field measurements of flow velocity made by Harvey et al. (2011) we judged that flow conditions are transitional and approach turbulent flow at a water slope of approximately 2E-05 when flow velocities are on the order of a centimeter per second. Such conditions are at the higher end of flow conditions that are commonly observed in the Everglades. Accordingly, we simplified our calculations by assuming a slope of 2E-05 for all calculations of *n*, which effectively presumes that *n* is not a function of flow velocity in the Everglades.

Table 1. Calibrated vegetation-specific drag coefficients for Sawgrass ridge, Eleocharis slough, and the floating aquatics Utricularia with attached periphyton in the Everglades. Calibrated values from Larsen et al. (2009)

Vegetation Class	**Vegetation-specific drag coefficients**		
	K_0	k	ζ
Sawgrass Ridge	$10^{2.12}$	1.38	
Eleocharis Slough	$10^{1.06}$	1.75	
Floating aquatic vegetation - Utricularia+periphyton			0.60

We used an alternative drag expression that performed better that eq. [3] for flow through dense floating aquatic vegetation (*Utricularia* sp.*)* with attached periphyton. Based on earlier work by Schutten and Davy (2000) and Vogel (1994), the alternative drag expression is:

$$C_d = \delta U^{-0.5} \qquad Eq. 7$$

where δ is an empirical coefficient. Larsen et al. (2009) identified a value of 0.6 for δ by fitting to field measurements of flow velocity in the presence of dense floating *Utricularia* and attached periphyton in Everglades National Park (Harvey et al., 2005). Also noted at the measurement site was abundant calcium carbonate minerals that had precipitated in the attached periphyton, a result of the water chemistry in many areas of the Everglades, which can add considerably to the flow resistance of the floating mat in Everglades sloughs. To generalize, we used a mean profile of floating *Utricularia* spp. with associated periphyton summarized from USGS measurements at several sites in the Everglades (Larsen et al., 2009). The mean

frontal area of the periphyton mat is thickest near the surface and declines exponentially with height until absent at approximately 30 cm below the water surface (Figure 4). The mat is assumed to float, thus, if the water depth is 80 cm, then the top 30 cm is assumed to host the floating mat whereas the bottom 50 cm of the water column only has emergent macrophytes. If water level changes the position of the floating mat moves up and down accordingly.

Following the steps as before, we substituted eq. [7] into eq. [2], rearranged, and then set the result equal to Manning's rate law, $U = \frac{1}{n} h^{\frac{2}{3}} S^1$, and then rearranged to solve for $n_{b\_periphyton}$, which yields:

$$n_{b_{periphyton}} = \frac{h^{\beta} S^{\alpha}}{U_{force\ balance}} = \frac{h^{\frac{2}{3}} S^1}{\left\{\frac{2gS}{\delta a}\right\}^{2/3}} \qquad Eq.8$$

When needed a combined roughness from floating periphyton and slough emergent vegetation was calculated using an averaging approach that assumes that roughness in the top 30 cm of the water column is dominated by floating aquatics with negligible contributions from emergent slough stems :

$$n_{b_{combined}} = \frac{h_{emergent}}{h} n_{b_{emergent}} + \frac{h_{periphyton}}{h} n_{b_{periphyton}} \qquad Eq.9$$

where h is the total water depth in the slough, $h_{periphyton}$ is 30 cm or is equal to h if h is less than 30 cm, and $h_{emergent}$ is $h - h_{periphyton}$ if $h > 30$ cm and 0 if h is ≤ 30 cm. Values of $n_{b\text{-}emergent}$ and $n_{b\text{-}periphyton}$ are depth-averaged roughness over the intervals $h_{emergent}$ and $h_{periphyton}$.

D-3. Normalizing ground elevations to assess microtopographic variation

Ross et al. (2015) provided measured water depths and absolute ground surface elevations at 8,568 locations. Here we aggregated the ground elevations by PSU and by sub-basin (Table 2).

Table 2. List of microtopography data clusters (PSUs) and number of measurements aggregated by sub-basin

Sub-basin	PSU ID	Number Microtopographic Observations
WCA-1	1, 17, 65	470
WCA-2A	9, 37, 61, 69, 73	698
WCA-2B	53	129
WCA-3A North	3, 11, 19, 27, 29, 51, 43, 67, 79	1,297
WCA-3A Central West	7, 23, 31, 39, 55, 71	1,036
WCA-3A Central East	15, 36, 45, 47, 63	770
WCA-3A South	26, 34, 52, 58, 66, 68	886
WCA-3B	13, 20, 28, 44, DPM, 220	1,142

ENP	0, 6, 10, 18, 22, 24, 30, 32, 513, 56, 62, BS1, BS2, BS3, 50, 54	2,140
	Total	8,568

To facilitate comparisons, we calculated a relative elevation at each point that factored out the large-scale trend in decreasing ground elevation from north to south in the Everglades. To calculate relative ground elevations, we normalized each ground elevation within a PSU by subtracting the median of all ground elevations in that PSU. The relative elevation for any observation is therefore the absolute ground elevation minus the median elevation of all ground elevations in that PSU:

$$RelElev_{point} = Abs\_Elev_{point} - PSU_{Median} \qquad Eq.\ 10$$

where,

$RelElev_{point}$ = relative ground surface elevation of a point comparable across PSUs

PSU_{Median} = median reference elevation within a PSU.

D-4. Associating microtopography and vegetation type

In this section we explain how ground elevations were associated with on the ground assessments of vegetation type. In Table 3 the many vegetation types reported by Ross et al. (2015) were simplified into four major vegetation classes, “Ridge”, “ Slough” encompassing common wet prairie vegetation in sloughs including the usual dominant Spikerush (*Eleocharis* sp.), Deepwater slough (where Water Lily, *Nuphar sp.,* is dominant and wet prairie specie are comparatively rare) and “Undefined Other” that included vegetation types that did not fit into the first three categories, e.g., vegetation in disturbed areas (e.g. Cattail) or areas not described as ridge and slough (e.g., Tree islands) that were not used in this analysis.

Table 3. Microtopography-associated observations of vegetation and classification as Ridge, Slough, Deepwater slough, and Undefined other categories. These three vegetation classes were used to combine the on-the-ground assignments of "Vegetation type" made at each topographic measurement site.

Ridge Class			Slough Class			Deepwater Slough Class			Undefined		
vege. Type	count	percent	vege. Type	count	percent	vege. Type	count	percent	vege. Type	count	percent
Ridge	4370	84.2%	Wet_Prairie	1006	83.4%	Slough	1463	100.0%	Bare_Area	1	0.1%
Ridge_slough	637	12.3%	Wet_Prairie_slough	49	4.1%				Cattail	227	31.9%
Ridge_Edge	27	0.5%	Slough_ridge	3	0.2%				Cattail_slough	6	0.8%
Ridge_Wet_Prairie	154	3.0%	Slough_wet_prairie	148	12.3%				Cattail_wet_prairie	13	1.8%
									Open_marsh	3	0.4%
									Ridge_Cattail	172	24.2%
									Ridge_TreeIsland	23	3.2%
									Rocky_ridge	2	0.3%
									Rocky_wet_prairie	1	0.1%
									Slough_cattail	12	1.7%
									Slough_Tree_Island	1	0.1%
									Tree_Island	88	12.4%
									TreeIsland_cattail	12	1.7%
									Tree_Island_ridge	2	0.3%
									Tree_Island_wet_prairie	2	0.3%
									Water	6	0.8%
									Wet_prairie_Tree_Island	5	0.7%
									Blank	135	19.0%
	5188	100%		1206	100%		1463	100%		711	100%
Percent		**60.6%**			**14.1%**			**17.1%**			**8.3%**

Table 4 reports the number and percentage of occurrence of each simplified vegetation class in each sub-basin. The cumulative distributions of relative ground elevation and the frequency distributions of ground elevation in each vegetation class are shown in Figure 5.

Table 4. Microtopography-associated estimation of Ridge, Slough, and Deepwater Slough areal coverage by sub-basin

Sub-Basin ID	Num_Ridge	Num_Slough	Num_DWS	% Ridge	% Slough	%DWS	% DWS+Slough
ENP	1594	469	22	76.5	22.5	1.1	23.5%
WCA-1	187	37	170	47.5	9.4	43.1	52.5%
WCA-3A North	766	174	105	73.3	16.7	10.0	26.7%
WCA-3A Central West	554	177	302	53.6	17.1	29.2	46.4%
WCA-2A	473	11	59	87.1	2.0	10.9	12.9%
WCA-3B	917	139	64	81.9	12.4	5.7	18.1%
WCA-3A Central East	224	21	420	33.7	3.2	63.2	66.3%
WCA-3A South	426	178	247	50.1	20.9	29.0	49.9%
WCA-2B	47	0	74	38.8	0.0	61.2	61.2%

D-5. Estimating characteristic ridge-slough microtopographic difference

We used sub-basin distributions of relative ground elevations to estimate a characteristic ridge-slough **microtopographic difference,** z_p. Researchers have estimated the difference in ground elevation between ridges and sloughs in various ways, including using the

standard deviation of elevations within a given area (e.g., Yuan and Cohen, 2017; Casey et al., 2016). Instead, we used breakpoints on the cumulative distribution of ground elevations in each sub-basin to help quantify z_p as the difference between the 90th percentile elevation that characterized ridge tops and an estimated no-flow threshold elevation that characterized the effective bottom of sloughs. The no-flow threshold elevation was approximated as the 10th percentile ground elevation, i.e., the elevation where lower elevations become increasingly rare and likely become too poorly connected to convey overland flow (Figure 5). Flow begins as water level rises above the no-flow threshold until eventually the sawgrass ridges become submerged, which was approximated as when water level exceeds the 90th percentile ground elevation.

A.

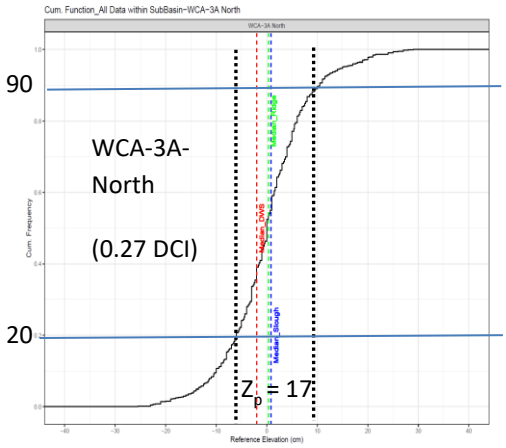

B.

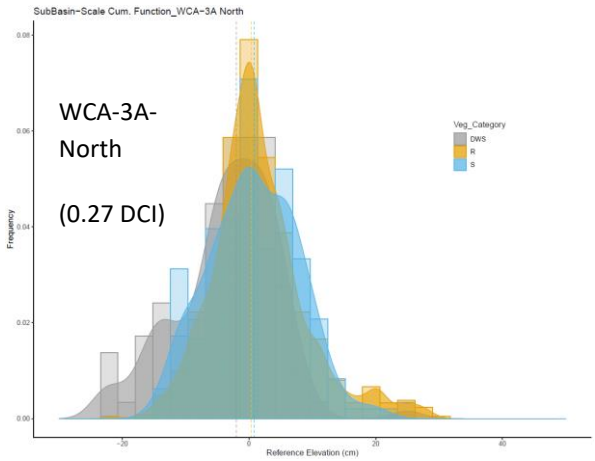

C.

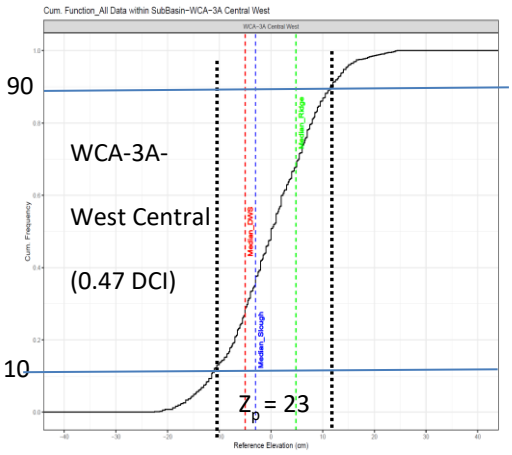

D.

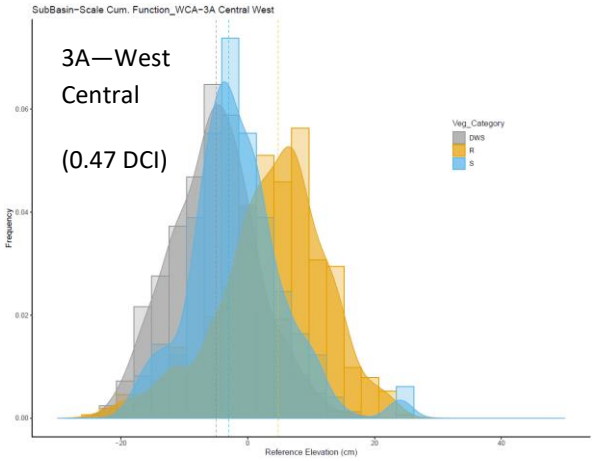

E.

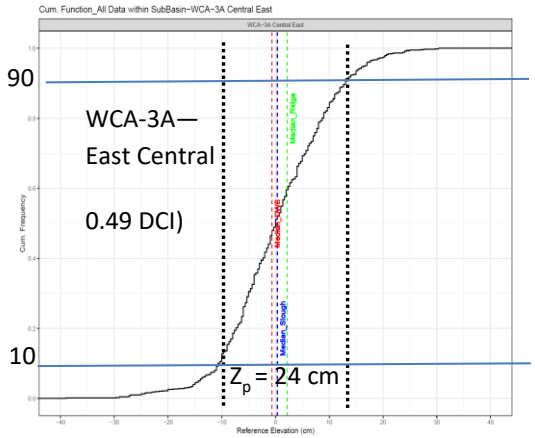
Cum. Function_All Data within SubBasin=WCA-3A Central East
90
WCA-3A—
East Central
0.49 DCI)
10
Z_p = 24 cm
Cum. Frequency
Reference Elevation (cm)

F.

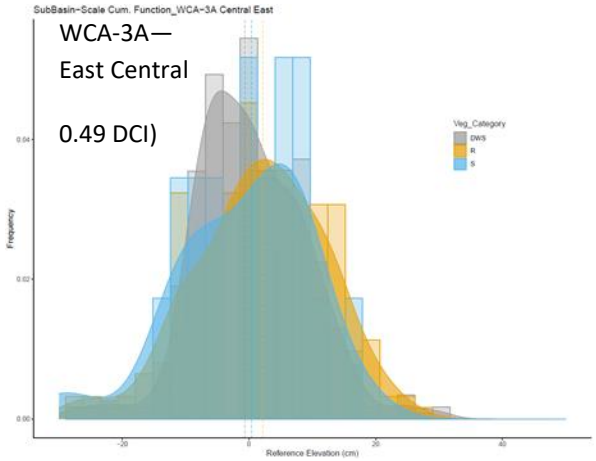
SubBasin-Scale Cum. Function_WCA-3A Central East
WCA-3A—
East Central
0.49 DCI)
Veg_Category
Frequency
Reference Elevation (cm)

G.

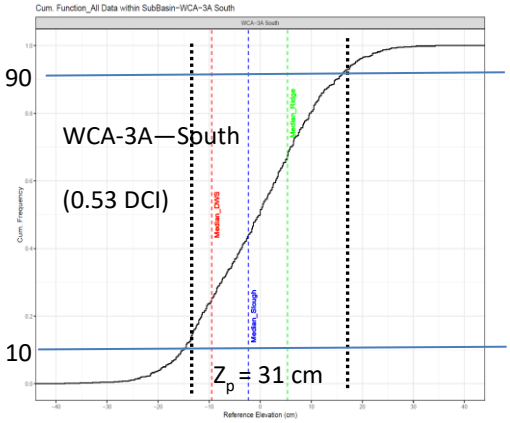
Cum. Function_All Data within SubBasin=WCA-3A South
90
WCA-3A—South
(0.53 DCI)
10
Z_p = 31 cm
Cum. Frequency
Reference Elevation (cm)

H.

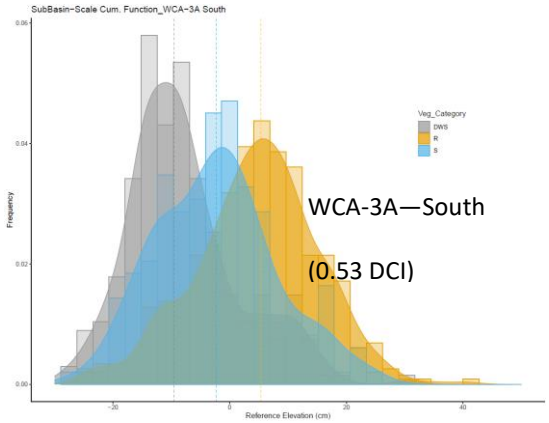
SubBasin-Scale Cum. Function_WCA-3A South
Veg_Category
WCA-3A—South
(0.53 DCI)
Frequency
Reference Elevation (cm)

I.

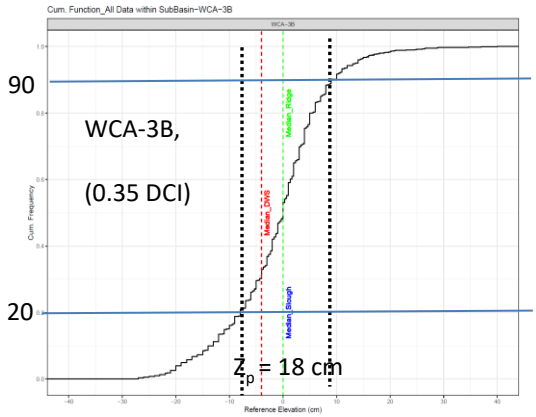
Cum. Function_All Data within SubBasin=WCA-3B
90
WCA-3B,
(0.35 DCI)
20
Z_p = 18 cm
Cum. Frequency
Reference Elevation (cm)

J.

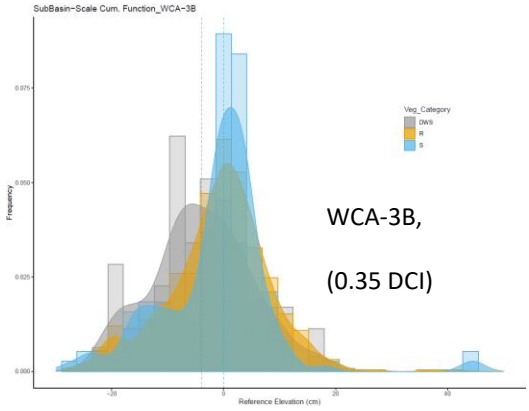
SubBasin-Scale Cum. Function_WCA-3B
Veg_Category
WCA-3B,
(0.35 DCI)
Frequency
Reference Elevation (cm)

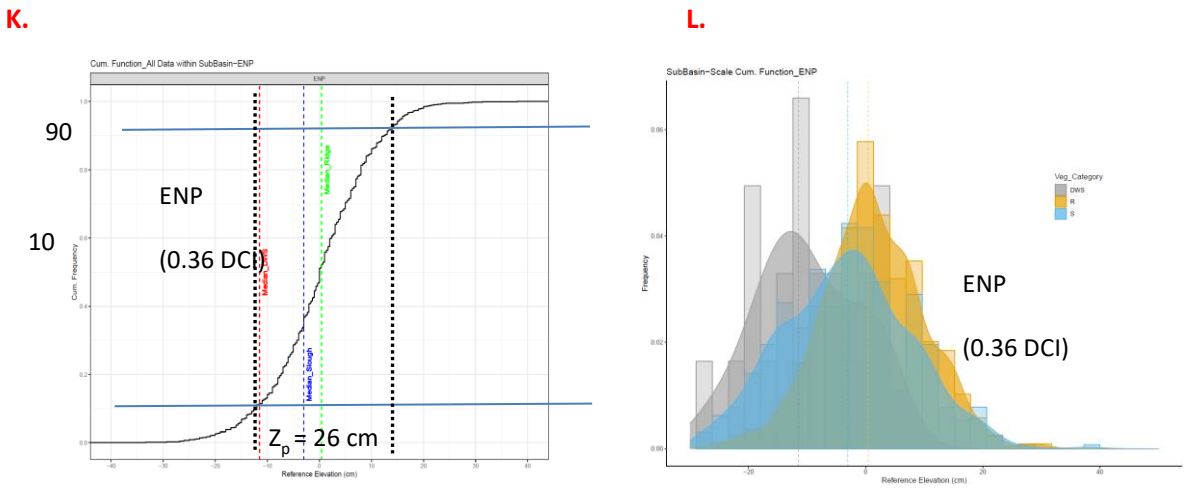

Figure 5. Cumulative distributions of relative microtopographic elevation (A, C, E, G, I, K) and frequency distributions of relative elevation by vegetation class, Ridge (orange), Eleocharis slough (blue), and Deepwater slough (grey) (B, D, F, H, J, L) for six sub-basins and vertical lines indicate the median of each vegetation class, WCA3A_North (A, B), WCA3A-West Central (C, D), WCA3A-East Central (E,F), WCA3A-South (G, H), WCA3B (I, J), and Everglades National Park (K, L).

Using the 10th percentile ground elevation as the no-flow threshold elevation was adequate for sub-basins where ridge proportion was relatively low and slough connectivity relatively high (i.e., $p \leq 0.7$ and DCI > 0.35). However, we noted that in sub-basins where ridge proportion was relatively high and slough connectivity relatively low (i.e., $p > 0.7$ and $DCI \leq 0.35$), the no-flow breakpoint occurred instead at the 20th percentile ground elevation. Using two criteria resulted in applying the 10th percentile ground elevation in the WCA-3A-West Central, WCA-3A-East Central, and WCA-3A-South sub-basins, and the 20th percentile elevation in the WCA-3A-North and WCA-3B sub-basins.

D-6. Analysis of vegetation maps to produce landscape pattern metrics

We selected 20 of the 49 vegetation maps (Ross et al., 2015: accessed by personal communication, February 2016) for analysis of landscape pattern in six sub-basins: WCA-3A-North, WCA-3A-Central West, WCA-3A-Central East, WCA-3B, WCA-3A-South, and ENP. We selected one or two sizeable circular areas of ridge and slough on each map where ridge-slough features were clear, i.e., where there were limited areas of other vegetation communities (e.g. cattail) or man-made structures (levees and canals). Both ridge- and-slough communities that were obviously in good condition, with a high degree of linear patterned features, or areas of ridge and slough that were substantially degraded were both deemed acceptable (Table 5).

Table 5. Forty-nine vegetation maps and 23 landscape pattern areas identified by associated PSU and sorted by sub-basin. The twenty map IDs selected for landscape pattern analysis are shown in red (* indicates that two 2-km circles were analyzed from a map instead of one), bringing the total analyses for landscape pattern to 23 area. All locations also shown on Figure 3

Sub-basin	PSU ID (red indicates used in landscape pattern analysis, * indicates 2 circles (2 -km diameter) analyzed from a single map)	Number of PSU
WCA-1	1, 17, 25, 33, 41	5
WCA-2A	5, 9, 21, 37	4
WCA-3A North	3, 11, 19, 27, 29, 35, 43	7
WCA-3A Central West	7, 23, 31, 39	4
WCA-3A Central East	15*, 36, 45, 47	4
WCA-3A South	2*, 4, 26, 34	4
WCA-3B	13, 20, 28, 44, DPM*, 108	6
ENP	0, 6, 8, 10, 14, 16, 18, 22, 24, 30, 32, 38, 40, 42, 46	15
	Totals	49 (23)

Circular areas as large as possible that fit the above criteria were delineated on each map, These sub setted areas typically had a diameter of ~ 2 km, which corresponds to a circle with an area of 6.3 km^2 (2.4 $mile^2$). Once delineated, the circles were cropped from the selected maps. Three of the twenty selected vegetation maps had enough area to analyze two circles of roughly equal size, and so twenty-three circular areas in total were selected for analysis (Appendix A).

Next, the mapped vegetation types in each circle were simplified by classifying mapped vegetation types into two categories, ridge and slough. Vegetation types other than ridge and slough comprised a low proportion of the landscape (approximately 8 %, Table 3), and those areas were even less common in the landscape pattern analysis because locations were avoided with significant undefined vegetation or manmade structures were avoided. The maps with simplified vegetation classes were then converted to a binary format delineating ridge and slough (Appendix A).

D-7. Landscape pattern analysis

The landscape pattern metrics and methods of analysis are briefly described in this section with references to the detailed method of analysis. Briefly, the four metrics (areal proportion of ridges, directional connectivity of sloughs, anisotropy of ridges, and fractal dimension of ridge-slough edge), were quantified at 23 locations across six sub-basins. Each sub-basin had between four and six of those locations, and landscape metrics were averaged

within each sub-basin to provide inputs for simulations using the biophysical flow rate expression (section F.)

D-7.1. Areal proportion of ridges

Areal proportion of ridges, *p*, estimates aerial coverage of ridges or sloughs at the km-scale using the sequential techniques of aerial photogrammetry and vegetation mapping (Ross et al., 2015; Rutchey et al., 2008), and processing to binarize images (Nungesser, 2011; Choi and Harvey, 2016; this paper) to delineate spatial patterns including areal proportion of ridges, *p.* Areal proportion of ridges was computed by counting the proportion of pixels in the image that were ridge as a percentage of the total number of pixels. The resulting estimate of the aerial proportion of ridges was compared with independent estimates of *p* based on the on-the-ground notations of vegetation type made at each of the thousands of randomly selected microtopography measurement points. Results were relatively consistent between those independent estimations of *p*. Here we used the vegetation map estimates of *p* in our subsequent analyses because to be consistent with the other calculated landscape pattern metrics which rely on the same subsetted vegetation maps from the indicated PSUs (Table 4 and Figure 3).

D7.2. Directional connectivity of sloughs

Directional connectivity of sloughs, *DCI*, used the twenty-three circular binarized landscape images described above to quantify the degree of continuity of uninterrupted pathways for flow through sloughs across a km-scale area with mixed ridges and sloughs. *DCI* is mathematically defined and quantified by the method outlined in Larsen et al. (2012) using the codes that are available at Environmental Systems Dynamics Laboratory (http://www.esdlberkeley.com). Briefly, DCI is computed as either a weighted or unweighted sum of the ratio of a projected distance along pixels tracing an uninterrupted pathway of slough between two nodes to the shortest path distance between the nodes, summed over all nodes and all projected distances. The weighting function emphasizes a particular length scale that is adjusted to account for limitations associated with map resolution or boundary effects. For this study we calculated both $DCI_{weighted}$ and $DCI_{unweighted}$. DCI is summarized as a maximum value and its compass direction relative to north. However, DCI is quantified for all directions and we provide those values for all compass directions in the associated data release (Harvey and Choi, 2022).

D-7.3. Anisotropy of ridges

Anisotropy of ridges, *e*, was quantified using the same twenty-three circular binarized images described above to quantify a shape factor that estimates the degree of elongation of ridges. For this study it was calculated using the equations and methods of Kaplan et al. (2012).

a. 1. Fractal dimension of ridge-slough c b. s

Fractal dimension of ridges, f_d, is based on estimation using the same twenty-three circular binarized images described above to quantify a measure of the spatial distribution of ridges that estimates the tendency for flow blocking by ridges resulting from their dense vegetation and slightly higher elevations that create tortuous flow pathways for water flowing through sloughs that must wind between the ridges. As used here, fractal dimension is defined and calculated using the "box-counting" method of Ronayne and Gorelick (2006) as applied in the Everglades and as discussed by Larsen et al. (2012).

E. Analysis Results

E-1. Roughness for single vegetation communities

Biophysical estimation of roughness is based in hydraulic theory of flow drag on emergent vegetation stems that protrude though shallow waters. The theory specifies how a wetland that has vegetation with many thinner stems causes more drag that slows the flow for a given driving force, i.e. water slope. A wetland with fewer thicker stems has lower roughness, less drag, and higher flow velocity for a given water slope. The biophysical estimation approach is distinguished from many previous studies where roughness is treated as an unmeasurable parameter that must be calibrated for every use. Biophysical estimation of roughness has the advantage of transferability to other locations and conditions without need for calibration to match hydrologic data.

Figure 6 summarizes the biophysical estimation of roughness for Sawgrass ridge, Deep-water slough, Spikerush slough, and Spikerush slough plus floating aquatics. Also illustrated is the sensitivity of roughness to variation in vegetation properties. The roughness bounds were produced by increasing or decreasing by 20% of the range the stem frontal area and stem diameter. The higher bound of roughness is created by a 20% increase in frontal area and a 20% decrease in stem diameter. The lower bound of roughness is the created by the opposite, i.e. a 20% of the range decrease in frontal area and a 20% of the range increase in stem diameter. The upper and lower bound estimates were used as inputs to a sensitivity analysis (section F.) to assess the dominant biophysical controls on overland flow.

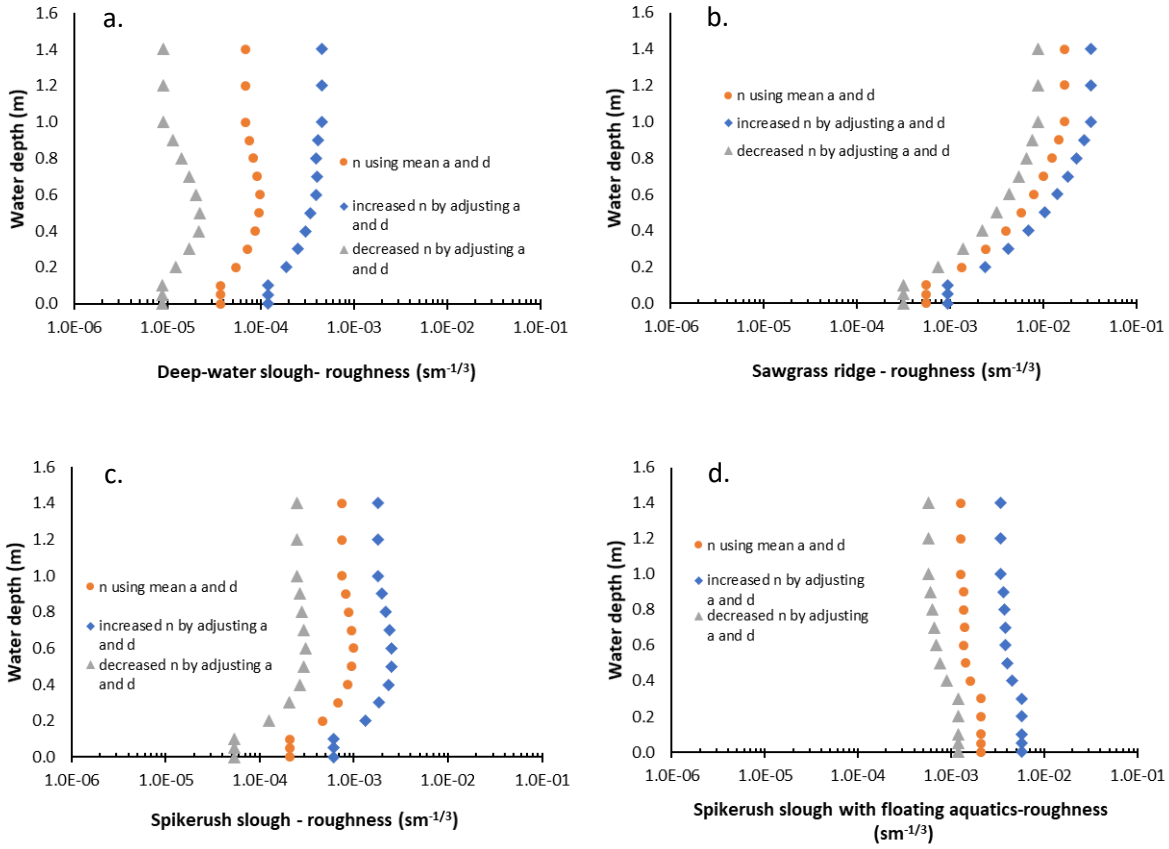

Figure 6. Mean roughness and upper and lower bound estimates for Deepwater slough (a), Sawgrass ridge (b), Spikerush slough (c), and Eleocharis slough with floating aquatics and periphyton (d). Mean roughness values (n_b) (orange symbols) were calculated as described in the text using stem frontal areas and diameters from Figure 4, and using vegetation-specific coefficients from Table 1, and a water slope of 2E10-5 and exponents on water depth and slope of 0.667 and 1, respectively. The higher and lower n_b values (blue and grey symbols, respectively) were estimated by decreasing *a* and increasing *d* by 20% of their range for higher roughness estimation, and vice versa to estimate lower roughness, for use in sensitivity analyses in section F-5.

E-1. Spatially averaged microtopography

Microtopography trends across the Everglades were summarized by aggregating the relative ground elevations by sub-basin. Each sub-basin had between one and sixteen PSUs and between 129 and 2,140 microtopographic observations within its boundaries (Table 2). The median, mean, standard deviation, and 10th, 20th, and 90th percentile relative ground elevations were computed for each sub-basin and are reported in Table 6. The relative ground elevations are normalized to a median ground elevation of zero. The standard deviation of relative ground elevations ranged from 8.8 to 15.5 cm, with the median of sawgrass ridges tending to be higher than the overall median, and sloughs tending to be lower (sawgrass ridges averaged 0.3 to 5.3 cm higher and deep-water sloughs averaged 0.7 to 11.5 cm lower than median ground elevation) (Table 6). The resulting estimates of z_p ranged from a low of 16.5 cm in WCA-3A-North to a high of 30.7 cm in WCA-3A-South (Table 6 and Figure 5).

Table 6. Everglades ridge and slough microtopographic variation summarized by sub-basin. Elevations are relative elevation, in centimeters, computed using equation 9. Statistics reported are for all elevations in a sub-basin or as broken down for three vegetation classes; Sawgrass ridge, Spikerush slough (Slough), and Deep-water Slough (DWS)

ID	ENP	WCA-1	WCA-3A North	WCA-3A Central West	WCA-2A	WCA-3B	WCA-3A Central East	WCA-3A South	WCA-2B
Mean_ALL	-1.0	-0.5	0.2	0.2	-1.3	-0.3	0.4	0.0	-0.3
Mean_Ridge	-0.2	3.2	1.6	3.8	0.9	-0.2	1.7	4.9	7.7
Mean_Slough	-3.9	-5.3	0.8	-1.8	-10.0	-0.9	-0.8	-2.1	#NUM!
Mean_DWS	-9.8	-8.2	-3.3	-5.3	-7.1	-4.0	0.2	-8.2	-6.7
Median_ALL	0.0	0.0	0.0	0.0	0.0	0.0	0.0	0.0	0.0
Median_Ridge	0.4	3.7	0.3	4.8	1.0	0.0	2.2	5.3	10.0
Median_Slough	-3.0	-5.0	0.8	-3.0	-10.7	0.0	0.3	-2.3	
Median_DWS	-11.5	-6.0	-2.0	-5.0	-7.3	-4.0	-0.7	-9.5	-9.5
SD_ALL	12.4	11.4	8.4	8.8	10.6	11.3	9.7	12.9	15.5
SD_Ridge	12.5	5.7	7.5	8.5	7.4	11.1	10.4	11.7	13.3
SD_Slough	12.2	13.3	7.0	7.3	9.0	10.9	10.5	11.4	
SD_DWS	8.8	10.4	8.0	6.8	8.2	8.8	9.0	10.1	13.2
All_Percentile_10	-14.0	-15.6	-10.0	-11.5	-13.3	-13.0	-10.7	-15.2	-19.3
All_Percentile_20	-8.0	-7.3	-6.0	-7.0	-8.0	-8.0	-7.3	-11.5	-16.1
All_Percentile_90	12.0	12.0	10.5	11.5	9.4	10.0	13.0	15.5	21.3
Microtopo. diff. z_p	26.0	27.6	16.5	23.0	22.7	18.0	23.7	30.7	40.6

E-3. Summary of landscape pattern and microtopography metrics

Landscape pattern metrics are summarized in Table 7. Included are 1) areal proportion of ridges, 2) slough directional connectivity index (DCI_W and DCI_U, weighted and unweighted, respectively, plus the direction of maximum DCI), 3) anisotropy of ridges, and 4) fractal dimension of ridges. Also included is the characteristic microtopographic difference between ridges and sloughs.

Table 7. Landscape pattern and microtopography metrics for the 23 selected Everglades locations shown in Figure 3 and enumerated in Table 4

Sub-basin	**Sub-basin Scale Metrics**			**Landscape Pattern Data Identifier (PSU)**	**Metrics Derived from Indicated PSU**						
	Z_p (cm)	***p*** (fraction)	***Max. DCI_W***	Binarized Vegetation Map PSU Identifier (file_ID name)	***Max. DCI_W***	***DCI_W* down-slope direction[1]**	***Max. DCI_U***	***DCI_U* down-slope direction[1]**	***e***	***p***	***f_d***
WCA-3A North	16.5	0.81	0.27	psu35_binary.txt	0.288	211.0	0.300	211.0	1.018	0.807	1.560
				psu43_binary.txt	0.253	122.6	0.286	122.6	1.046	0.810	1.467

WCA-3A Central West	23.0	0.59	0.47	psu7_binary-1.txt	0.578	165.2	0.613	165.2	1.019	0.653	1.638
				psu23_binary.txt	0.435	167.6	0.521	167.6	1.036	0.584	1.684
				psu31_binary.txt	0.216	174.4	0.270	174.4	1.038	0.715	1.491
				psu39_binary.txt	0.641	189.4	0.646	189.4	1.062	0.413	1.847
WCA-3A Central East	23.7	0.41	0.49	psu15_binary-1.txt	0.246	106.2	0.283	110.2	1.117	0.642	1.502
				psu15_binary-2.txt	0.593	211.2	0.590	211.2	1.376	0.286	1.892
				psu36_binary.txt	0.696	258.5	0.693	170.5	1.081	0.216	1.925
				psu45_binary.txt	0.408	108.2	0.440	120.2	1.487	0.506	1.670
WCA-3A Central South	30.7	0.44	0.53	psu2_binary-1.txt	0.660	168.3	0.664	168.3	1.106	0.375	1.835
				psu2_binary-2.txt	0.657	176.3	0.662	176.3	1.071	0.307	1.877
				psu26_binary.txt	0.380	190.4	0.430	190.4	1.137	0.554	1.697
				psu34_binary.txt	0.438	190.8	0.465	190.8	1.074	0.515	1.642
WCA-3B	18.0	0.88	0.35	psu20_binary.txt	0.456	115.5	0.430	115.5	1.007	0.948	1.052
				psu28_binary.txt	0.414	125.1	0.391	127.1	1.009	0.919	1.160
				psu44_binary.txt	0.289	124.3	0.302	124.3	1.018	0.879	1.237
				dpm_binary-1.txt	0.298	179.4	0.320	179.4	1.049	0.835	1.385
				dpm_binary-2.txt	0.284	267.4	0.302	159.4	1.062	0.820	1.399
ENP	26.0	0.7	0.36	psu0_binary.txt	0.358	178.0	0.408	197.99	1.042	0.651	1.588
				psu18_binary.txt	0.359	205.8	0.406	210.8	1.077	0.581	1.712
				psu30_binary.txt	0.426	248.7	0.440	241.76	1.028	0.706	1.570
				psu32_binary.txt	0.301	155.0	0.303	155.0	1.004	0.842	1.385
Statistics	***23.0***	***0.64***	***0.41***	***Mean***	*0.42*	*175.6*	*0.44*	*168.7*	*1.09*	*0.63*	*1.57*
				Standard Deviation	*0.15*	39.54	0.14	33.70	0.12	0.21	0.23

notations - [1] - Down-slope directions in degrees clockwise from north clockwise are reported for the maximum values of DCI. Downs-lope direction assumes that the regional ground surface slopes in a direction between 90 and 270 degrees.

F. Flow simulation inputs and hydrologic data for comparisons

A limitation of biophysical modeling using stem architecture from a single vegetation community, as outlined in section D., is that it only applies where vegetation is homogeneous and growing on level ground. Consequently, it has limited use in wetlands where several vegetation communities are present and may occupy slightly higher or lower ground. Such heterogeneity is typical in wetlands, and it is pronounced in the Everglades (Kadlec and Knight, 1996; Choi and Harvey, 2013). A concerted effort has been made by researchers to make use of biophysical data to improve overland flow modeling in the Everglades (Harvey et al., 2009; Lal et al., 2015; Larsen et al., 2017; Lal, 2020).

Here we employed upscaling theory to facilitate larger scale applications with spatially varying vegetation and topography. We followed Larsen et al.'s (2017) spatial power averaging approach that uses geostatistical methods of spatial power averaging to estimate *effective* parameters for large-scale wetland models where cell sizes are 1 km^2 or larger. Upscaling blends the influence of differing microtopography and vegetation drag in sloughs and ridges to estimate area-averaged discharge through the ridge and slough landscape. The characteristic microtopographic difference, z_p, approximates the height of ridge tops above the slough bottom and h characterizes the water depth in sloughs such that h - z_p is the water depth on ridges. When water level is relatively high and above the ridge tops, i.e., $h > Z_p$, the upscaled biophysical rate expression is:

$$q(h) = \left\{\left[p\left(K_R\left(h - z_p\right)\right)^{\omega} + (1-p)(K_S h)^{\omega}\right]^{\frac{1}{\omega}}\right\}^{\frac{5}{3}} \cdot S^{1.0} \;=\; K_{eff} h_{eff}\, S^1 \qquad Eq.11$$

and when ridges become dry, e.g., when $h \le Z_{p,}$ the rate expression is:

$$q(h) = \left\{[(1-p)(K_S h)^{\omega}]^{\frac{1}{\omega}}\right\}^{\frac{5}{3}} \cdot S^{1.0} \;=\; K_{eff} h_{eff}\, S^1 \qquad Eq.12$$

where $q(h)$is the spatially averaged and depth average discharge per unit width (L^2/T) through the ridge and slough landscape, h is a characteristic water depth relative to height where flow starts (approximately the slough bottom); S = water slope; z_p is the characteristic elevation difference between ridge and slough, p = ridge proportion (unitless); ω = fitted spatial power averaging exponent (unitless), K_R is the biophysical conductance coefficient for ridges and K_R is for sloughs, i.e., K is equivalent to the biophysical roughness coefficient (from eq. [6]) for slough, n_s, or ridge, n_r, raised to the power -3/5; and K_{eff} and h_{eff} are the effective (i.e.,

upscaled) values of *K* and *h* that account for the blending of ridge and slough and the associated landscape factors. Although the equations are written in terms of the conductance coefficient *K,* for this study we report values of *n* rather than *K* because of the familiarity of a roughness formulation from Manning's equation in the overland flow literature.

We estimated the spatial averaging coefficient ω for our simulations using measured values of the landscape aerial proportion of sawgrass ridge (*p)*, the difference in ground surface height of ridges and sloughs (z_p), the directional connectivity of sloughs (*DCI*) (Larsen et al., 2012), anisotropy (*e*) (Kaplan et al., 2012), and fractal dimension (f_d) (Li et al., 2009). To calculate ω the values of those metrics were used as inputs to Larsen et al.'s (2017) multiple regression models that predicted ω as a function of *h*, z_p, *p, DCI, e,* and f_d based on fitting of multiple regression models to match outputs from 11,760 simulations of a 2-dimensional numerical model of overland flow that represented various landscape configurations and water levels (Larsen et al., 2017).

All of the data inputs to equations [10] and [11] are provided in Harvey and Choi (2022), including the spatial averaging exponent ω. The spatial averaging coefficient ω was calculated using Larsen et al.'s (2017) multiple regression equations for three classes of water surface stage:

1) high water conditions with $h \geq Z_p + 15$ cm

2) low water conditions with $h \leq Z_p$, and

3) transitional surface water stages with $Z_p < h < Z_p + 15$ cm.

The solutions for ω across the three classes of surface water stage are provided below, beginning with the high-water case ($h \geq Z_p + 15$ cm), where ω_H is specified by:

$$\omega_H = m\left(h - z_p\right) + b \qquad Eq. 13$$

where *m* is specified by the following multiple regression equation:

$$m = 523 - 284f_d - 543P^{-0.29} + 0.35e + 300f_d \cdot P^{-0.28} - 0.16e \cdot f_d - 39P^{14.6}e + 32P^{16.6} \cdot e \cdot f_d \qquad Eq.\ 14$$

and b is specified by:

$$b = -9.83 + 0.53\ln(e) + 2.34P + 4.76f_d - 4.06(P - 0.5) \cdot (f_d - 1.77) + 0.19\ln(DCI) - 0.09\ln(DCI) \cdot \ln(e). \qquad Eq.\ 15$$

where, for clarity we again define *DCI* as the multi-scale, unweighted Directional Connectivity Index calculated for sloughs according to the method of Larsen et al. (2012), f_d is fractal

dimension calculated using the method of (Li et al., 2009), and *e* is the anisotropy calculated using the method of Kaplan et al. (2012).

For cases where $h = z_p$ and $h \leq z_p$, ω is specified either as ω_{Zp} or ω_L, respectively, where ω is calculated using the appropriate multiple regression equation below:

$$\omega_{Zp} = 0.14 + 0.22DCI + 0.25P - 0.65(P - 0.4) \cdot (DCI - 0.38) + 0.14\ln(e) - \ 0.14\ln(e) \cdot (P - 0.4) \quad Eq.16$$

or

$$\omega_L = -0.08 + 0.55P + 0.45DCI - 1.52(P - 0.35) \cdot (DCI - 0.47) + 0.08\ln(e) - 0.36\ln(e) \cdot (P - 0.35) \quad Eq.17$$

where the variables are previously defined.

Between the high and low water conditions ($Z_p < h < Z_p + 15$ cm) the transitional value of the weighting factor, ω_T, is calculated as a linear interpolation:

$$\omega_T = \frac{\omega_H^* - \omega_{Zp}}{15}\left(h - z_p\right) + \omega_{Zp} \quad Eq.18$$

where ω_H^* is ω_H calculated at $h = z_p + 15$cm.

In the remainder of section F, we explain how we used measured vegetation, microtopography and landscape pattern metrics to compute overland flow for selected areas of the Everglades. In brief, we parameterized two classes of biophysical simulations for the Everglades, referred to as *Bio*FRE, which stands for biophysical flow rate expression. Each simulation uses Larsen et al.'s (2017) upscaled rate law (equations 10 and 11) from the actual Everglades. For each simulation the spatial averaging coefficient was computed for increments of water level using equations 12 -17.

The first set of simulations (*Bio*FRE-NSM) was for historicalal Everglades conditions based on hindcasted knowledge as well as representative measurements of vegetation communities, microtopography and landscape conditions in the present-day. *Bio*FRE-NSM was compared with the Natural System Regional Simulation Model (Said and Brown, 2013).

The second set of simulations (*Bio*FRE-sub-basin) were for six sub-basins in the present-day Everglades conditions where model inputs were based on present-day measurements discussed in section D. The present-day simulations also formed the basis for a sensitivity analysis to identify the dominant biophysical controls on overland flow in the Everglades.

F-1. NSRSM simulations of historical Everglades overland flow

The Natural Systems Regional Simulation Model (NSRSM ver. 3.5.2; Said and Brown, 2013) provided simulations of flow versus water depth for historicalal, pre-drainage Everglades. Here we summarize their simulations for the northern, central, and southern Everglades, which are named NSRSM 512-sawgrass plains, 511-ridge and slough, and 514-ridge and slough south, respectively. NSRSM authors calibrated their simulations to reproduce approximate water depths that support the vegetation communities that were known to be present from photographs and historicalal accounts in the early twentieth century Everglades (McVoy et al., 2011).

F.2 *Bio*FRE-NSM simulations of historical Everglades overland flow

A biophysical flow rate expression *Bio*FRE-NSM was adapted from biophysical theory (Larsen et al., 2017) to estimate flow through the historicalal Everglades ridge and slough wetlands. *Bio*FRE-NSM simulations are not calibrated – rather they are parameterized based on inferred ridge and slough vegetation community types, microtopography, and landscape pattern metrics such as "slough connectivity". Input parameter values are based on historicalal accounts (McVoy et al., 2011) and modeling of the evolution of ridge and slough landscapes by Larsen and Harvey (2011). Four Natural System Model (NSM) cases were simulated for benchmarking against the NSRSM simulations described above: *Bio*FRE-NSM-DWS (Deep-water slough) dominated by Water Lily, a possible analog for the historical southern Everglades; *Bio*FRE-NSM-SS (Sparse Spikerush slough), a possible analog for the historical central Everglades; *Bio*FRE-NSM-DS (Dense Spikerush slough) which represents the mean stem architecture of present-day Spikerush sloughs, and a possible analog for a degrading natural system, and *Bio*FRE-NSM-SP (Sawgrass Plains) which represents the mean condition of Sawgrass ridges on a landscape dominated by sawgrass (p = 0.88), and a possible analog for the historical northern Everglades. *Bio*FRE-NSM simulation inputs are summarized in Table 8.

Table 8. *Bio*FRE-NSM input parameters for simulations of natural system overland flows in the Everglades. The simulations were parameterized as a function of vegetation community, landscape characteristics and water level. Vegetation roughness is reported for only a single water depth, 40 cm, because it varies continuously with water level.

Simulation Name / ***Parameters***		***Bio*FRE-NSM-SP** Sawgrass Plain	***Bio*FRE-NSM-SS** Sparse Spikerush in sloughs	***Bio*FRE-NSM-DWS** Deep Water Slough	***Bio*FRE-NSM_DS** Dense Spikerush Slough	***Bio*FRE-NSM-DSP** Dense Spikerush w/ periphyton on floating aquatics
Landscape	*Possible analog for*	Historical Northern Everglades	Historical Central Everglades	Historical Southern Everglades	Degrading natural system	Degrading natural system
	p	0.880	0.421	0.421	0.421	0.421
	DCI_w	0.35	0.533	0.533	0.533	0.533

	DCI_u	0.35	0.556	0.556	0.556	0.556
	f_d	1.247	1.777	1.777	1.777	1.777
	z_p (cm)	45.0	45.0	45.0	45.0	45.0
Vegetation	*Slough vegetation*	water-lily with sparse floating aquatics	sparse spikerush invasion	dense spikerush invasion	dense spikerush with calcareous periphyton on floating aquatics	mixed spikerush/sawgrass invasion
	Slough roughness n_{s_40cm} [$m^{-1/3}s$]	8.648E-04	2.675E-04	8.738E-05	8.648E-04	1.600E-03
	Ridge roughness n_{r_40cm} [$m^{-1/3}s$]	3.974E-03	3.974E-03	3.974E-03	3.974E-03	3.974E-03

F-3. *Bio*FRE-"sub-basin" simulations of present-day Everglades overland flow

*Bio*FRE-"sub-basin" simulations were parameterized based on measured vegetation, microtopography, and landscape pattern to represent conditions ranging from relatively well functioning but degrading, to poor-functioning but potentially restorable ridge and slough. The present-day simulations were compared with observed hydrologic data as well as with the NSRSM and *Bio*FRE-NSM simulations. Six present-day cases were simulated: *Bio*FRE-3Anorth, 3Awest, 3Aeast, 3Asouth, 3B, and ENP, named for the sub-basins they represent, respectively, WCA3A-North, WCA-3A Central East, WCA-3A Central West, WCA-3B, and Everglades National Park (ENP). *Bio*FRE-sub-basin simulation inputs are summarized in Table 9.

Table 9. *Bio*FRE input parameters for simulations of present-day overland flows in sub-basins of the Everglades. The simulations were parameterized as a function of vegetation community, landscape characteristics and water level. Vegetation roughness is reported for only a single water depth, 40 cm, because it varies continuously with water level.

Simulation Name / ***Parameters***		*Bio*FRE-3Anorth	*Bio*FRE-3Awest	*Bio*FRE-3Aeast	*Bio*FRE-3Asouth	*Bio*FRE-3B	*Bio*FRE-ENP
landscape	p	0.81	0.55	0.41	0.44	0.88	0.65
	DCI_w	0.27	0.55	0.49	0.56	0.35	0.38
	DCI_u	0.29	0.59	0.49	0.56	0.35	0.42
	f_d	1.513	1.723	1.772	1.765	1.247	1.623
	z_p (cm)	16.5	23.0	23.7	30.7	18.0	26.0
Ve	*slough vegetation*	dense spikerush	dense spikerush	dense spikerush	dense spikerush	dense spikerush	dense spikerush

	n_{s_40cm} [$m^{-1/3}s$]	8.648E-04	8.648E-04	8.648E-04	8.648E-04	8.648E-04	8.648E-04
	n_{r_40cm} [$m^{-1/3}s$]	3.974E-03	3.974E-03	.974E-03	3.974E-03	3.974E-03	3.974E-03

F-4. *Bio*FRE "well" and "poor" base cases to assess dominant biophysical controls

Two base cases for sensitivity testing of biophysical controls of overland flow were prepared. First was the *Bio*FRE-well-degrading base case that was set up to simulate a relatively well functioning but degrading ridge and slough landscape. Second was the *Bio*FRE-Poor-restoring base case that was set up for simulating a poor functioning but potentially restorable ridge and slough. Base cases for sensitivity testing are described in Table 10.

Table 10. Base cases for assessing sensitivity of overland flow and relative importance of controls. Parameter values are given for two base cases, 1) BioFRE-well, a present-day, well-functioning landscape, and 2) BioFRE-poo, a present-day, poor-functioning landscape based on selections of vegetation, microtopography, and landscape pattern inputs as described in the text.

	Base cases / Parameters	***Bio*FRE-well**	***Bio*FRE-poor**
Landscape Pattern Metrics	***Aerial proportion ridges, p***	**0. 421**	**0.846**
	Directional Connectivity Index for sloughs, DCI_w	**0.533**	**0.309**
	Directional connectivity index for sloughs, DCI_u	**0.556**	**0.328**
	Fractal dimension of ridges, f_d	**1.795**	**1.354**
	Microtopographic variation, Z_p (cm)	**30**	**15**
Vegetation Metrics	***Roughness*** *for sawgrass ridge,* n_{ridge} [$m^{-1/3}s$]	n_{15cm} = **0.0009** n_{40cm} = **0.0040** n_{65cm} = **0.0089**	n_{8cm} = **0.0006** n_{25cm} = **0.0019** n_{50cm} = **0.0058**
	Roughness *for "DS", dense spikerush slough,* n_s [$m^{-1/3}s$]	n_{15cm} = **0.0003** n_{40cm} = **0.0009**	

		n_{65cm} = **0.0010**	
	Roughness *for "DSP", dense spikerush + periphyton mat slough,* n_S [$m^{-1/3}s$]		n_{8cm} = **0.0021** n_{25cm} = **0.0021** n_{50cm} = **0.0014**
Water slope		**2E-05**	**2E-05**
Coefficients		α = **0.667;** β = **1;** K_o and k from Table 1	α = **0.667;** β = **1;** K_o and k from Table 1

F-5. *Bio*FRE sensitivity testing to assess dominant biophysical controls of overland flow

The two base cases of *Bio*FRE were prepared for sensitivity testing by perturbing Input parameters of each base case by 20% of the range, one by one, followed by rerunning the simulation to estimate sensitivity. The *Bio*FRE-Well simulation tested sensitivity in a direction of degrading landscape function (e.g., input parameters were perturbed in a direction that was thought to lower overland flow). The *Bio*FRE-Poor simulation tested sensitivity in a direction of restoring function (e.g., input parameters were perturbed in a direction that was thought to increase overland flow). Sensitivities were tested at three depths: 15, 40 and 65 cm for the *Bio*FRE-Well test and 8, 25, and 50 cm for the *Bio*FRE-Poor test. Parameter perturbations for Well and Poor functioning base cases are given in Table 11 and Table 12, respectively.

Table 11. Landscape parameters and model inputs for *Bio*FRE-Well-degrading sensitivity test

	SIMULATION PARAMETERS	base case ***Bio*FRE-Well**	degraded by **landscape pattern (*p*, *DCI*, and/or f_d)**	degraded by **vegetation roughness (*n*)**	degraded by **microtopography (z_p)**
Landscape Parameters	***p***	*p* = 0.421	*p* = **0.567**	*p* = 0.421	*p* = 0.421
	***DCI*$_w$**	DCI_w = 0.533	DCI_w = **0.456**	DCI_w = 0.533	DCI_w = 0.533
	***DCI*$_u$**	DCI_u = 0.556	DCI_u = **0.477**	DCI_u = 0.556	DCI_u = 0.556
	f_d	f_d = 1.795	f_d = **1.643**	f_d = 1.795	f_d = 1.795
	z_p (cm)	z_p = 30.0	z_p =30.0	z_p =30.0	z_p = **24.0**
Vegetation Parameters	n_r (Mean Sawgrass ridge)	Sawgrass ridge, computed with mean, depth-dependent *a* and *d* and water slope =2 E-05	same as base case	perturbed by increasing *a* by 20% or range and decreasing *d* by 20% of range n_{15cm}= 0.0017	same as base case

	($m^{-1/3}s$)	n_{15cm} = 0.0009 n_{40cm} = 0.0040 n_{65cm} = 0.0089	n_{15cm}= 0.0009 n_{40cm} = 0.0040 n_{65cm} = 0.0089	n $_{40cm}$ = 0.0070 n_{65cm} = 0.0163	n_{15cm}= 0.0009 n_{40cm} = 0.0040 n_{65cm} = 0.0089
	n_s (Dense Spikerush slough) ($m^{-1/3}s$]	Dense spikerush slough, computed with mean, depth-dependent *a* and *d* for dense spikerush slough w/ periphyton and water slope =2 E-05 n_{15cm} = 0.0003 n_{40cm} = 0.0009 n_{65cm} = 0.0010	same as base case n_{15cm}= 0.0003 n_{40cm} = 0.0009 n_{65cm} = 0.0010	perturbed by decreasing *a* by 20% or range and increasing *d* by 20% of range n_{15cm}= 0.0010 n_{40cm} = 0.0023 n $_{65cm}$ = 0.0025	same as base case n_{15cm}= 0.0003 n_{40cm} = 0.0009 n_{65cm} = 0.0010

Table 12. Landscape parameters and model inputs for *Bio*FRE-Poor-restoring sensitivity test

	Simulations Parameters	base case ***Bio*FRE-Poor**	improved by **landscape pattern (*p*, *DCI*, and/or f_d)**	improved by **vegetation roughness (*n*)**	improved by **microtopography (z_p)**
Landscape Parameters	***p***	*p* =0.846	*p* = **0.70**	*p* = 0. 846	*p* = 0. 846
	DCI_w	DCI_w = 0.309	DCI_w = **0.386**	DCI_w = 0. 309	DCI_w = 0. 309
	DCI_u	DCI_u = 0.328	DCI_u = **0.407**	DCI_u = 0. 328	DCI_u =0. 328
	f_d	f_d = 1.354	f_d = **1.506**	f_d = 1. 354	f_d = 1. 354
	z_p (cm)	z_p = 15.0	z_p = 15.0	z_p = 15.0	z_p = **18**
Vegetation Parameters	***n_r*** (Mean Sawgrass ridge) ($m^{-1/3}s$)	Sawgrass ridge, computed with mean, depth-dependent *a* and *d* for sawgrass and water slope =2 E-05 n_{8cm}=0.0006 n_{25cm}=0.0019 n_{50cm}=0.0058	same as base case n_{8cm}=0.0006 n_{25cm}=0.0019 n_{50cm}=0.0058	perturbed by decreasing *a* by 20% or range and increasing *d* by 20% of range n_{8cm}=0.0003 n_{25cm}=0.0011 n_{50cm}=0.0032	same as base case n_{8cm}=0.0006 n_{25cm}=0.0019 n_{50cm}=0.0058
	n_s (Dense Spikerush	Dense spikerush slough with floating aquatics and attached periphyton, computed with mean, depth-	same as base case	perturbed by decreasing *a* by 20% or range and increasing *d* by 20% of range	same as base case

	slough with Periphyton) [$m^{-1/3}s$]	dependent *a* and *d* for dense spikerush and water slope =2 E-05 n_{8cm}=0.0021 n_{25cm}=0.0021 n_{50cm}=0.0014	n_{8cm}=0.0021 n_{25cm}=0.0021 n_{50cm}=0.0014	n_{8cm}=0.0012 n_{25cm}=0.0012 n_{50cm}=0.0008	n_{8cm}=0.0021 n_{25cm}=0.0021 n_{50cm}=0.0014

Perturbations of the input parameters were standardized but also respected the inherent parameter correlations. Areal ridge proportion and microtopographic difference were perturbed by 20% of their range. The landscape pattern metrics that were strongly correlated with ridge areal proportion, i.e., directional connectivity and fractal dimension, were perturbed based on a 20% perturbation of *p* and the associated value of the landscape pattern metric using the linear regressions shown in Figure 7. Because of the generally high correlations between landscape pattern variables, the sensitivity of landscape pattern metrics was tested together as a whole, by perturbing ridge areal proportion, directional connectivity, and fractal dimension as one parameter. Each landscape pattern metric was also tested individually.

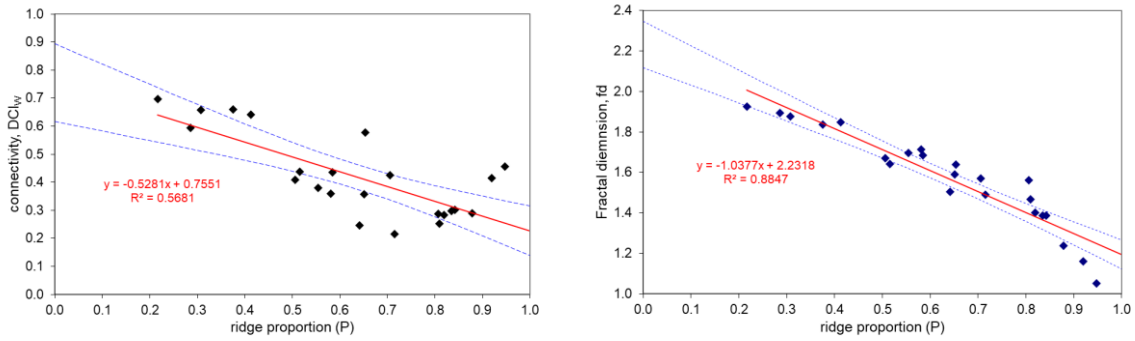

Figure 7. Linear regression of landscape pattern metrics DCI_w and f_d on areal ridge proportion, *p*. In comparison, ridge anisotropy was relatively poorly related with *p*.

The perturbations of input variables for sensitivity testing of *Bio*FRE Well and *Bio*FRE Poor were in one direction only. For example, perturbations for *Bio*FRE Well, which was intended to identify dominant biophysical variables causing degradation, were in a direction hypothesized to decrease overland flow relative to its base case. On the other hand, the *Bio*FRE Poor sensitivity test was intended to identify the dominant biophysical controls on restoration, and therefore the perturbations of input variables were in a direction thought to increase overland flow.

E-2. Hydrologic observations to compare with simulations

Hydrologic data including observations of water depth, slope, flow velocity, discharge, and conveyance were obtained from published data at 5 locations in four sub-basins of the Everglades. The sites represent conditions in WCA-3A Central East (1 site), WCA-3A Central

West (1 site), WCA-3B (1 site), and Everglades National Park (ENP, 2 sites). All hydrologic data are provided in Table 13.

Table 13. Hydrologic observations of overland flow at five sites in the Everglades, including water slope, water depth, water velocity, water discharge, and conveyance

Sub Basin	Site	Ref	Vege-tation		Date of Obser-vation	Water Slope	Water Depth (m)	Relative Water Level (m)	Ridge Velocity V_R_obs (cm/s)	Slough Velocity V_S_obs (cm/s)	*PSU*	*P, ridge frac-tion*	Average Velocity V_obs (cm/s)		Unit-width Discharge $q_{\_obs}$ (m2/s)	Convey-ance C_{obs} (m^2/s)
WCA -3A CW	3A-5	1	ridge/ slough		8/15/06	2.3E-05	0.48	0.37	0.530	0.530	31	0.591	0.53		2.5E-03	111
	3A-5	1	ridge/ slough		10/15/06	2.0E-05	0.58	0.47	0.450	0.460	31	0.591	0.46		2.7E-03	133
	3A-5	1	ridge/ slough		11/15/06	1.5E-05	0.70	0.59	0.330	0.420	31	0.591	0.42		2.9E-03	196
	3A-5	1	ridge/ slough		12/15/06	1.1E-05	0.44	0.33	0.180	0.300	31	0.591	0.30		1.3E-03	126
WCA -3B	RS1	2	ridge/ slough		12/15/15	5.1E-04	0.57	0.49			DP M1	0.835	3.10		1.8E-02	35
	RS1	2	ridge/ slough		12/15/15	3.0E-05	0.40	0.32			DP M1	0.835	0.30		1.2E-03	40
	RS1	2	ridge/ slough		12/15/15	1.7E-04	0.63	0.55	2.20	3.04	DP M1	0.835	3.02		1.9E-02	113
	RS1	2	ridge/ slough		12/15/15	2.0E-05	0.50	0.42	0.15	0.36	DP M1	0.835	0.36		1.8E-03	90
	RS1	2	ridge/ slough		12/10/13 - 12/19/13	2.2E-04	0.60	0.52	2.34	3.57	DP M1	0.835	3.54		2.2E-02	96
	RS1	2	ridge/ slough		11/24/15 - 12/3/15	1.6E-04	0.57	0.49	2.82	3.37	DP M1	0.835	3.36		1.9E-02	119
	RS1	2	ridge/ slough		11/15/16 - 11/24/16	1.9E-04	0.62	0.54	1.31	1.82	DP M1	0.835	1.81		1.1E-02	59

	RS1	2	ridge/ slough		12/10/16 - 12/19/16	1.6E-04	0.59	0.51	1.19	3.74	DP M1	0.835	3.68		2.2E-02	137
	RS1	2	ridge/ slough		1/1/13 - 1/30/13	4.9E-06	0.44	0.36	0.27	0.58	DP M1	0.835	0.58			
	RS1	2	ridge/ slough		9/18/14 - 10/17/14	1.3E-05	0.47	0.39	0.03	0.52	DP M1	0.835	0.52		2.5E-03	186
	RS1	2	ridge/ slough		2/11/17 - 3/17/17	7.7E-06	0.36	0.28	0.52	0.53	DP M1	0.835	0.53			
ENP	G-203	3	ridge only		1/5/01	4.0E-05	0.24	0.36	0.59	N/A	32	0.842	0.59		1.4E-03	35
	G-203	3	ridge only		8/15/01	4.0E-05	0.25	0.37	0.96	N/A	32	0.842	0.96		2.4E-03	60
	G-203	3	ridge only		11/1/01	4.6E-05	0.53	0.65	1.29	N/A	32	0.842	1.29		6.8E-03	149
	G-203	3	ridge only		2/1/02	3.7E-05	0.20	0.32	0.66	N/A	32	0.842	0.66		1.3E-03	36
WCA-3ACE	CA311	4	ridge/ slough		7/15/02	2.0E-05	0.61	0.50	1.25	1.78	31	0.41	1.77		1.1E-02	543
	CA311	4	ridge/ slough		2/1/02	2.0E-05	0.385	0.28	0.6	0.4	31	0.41	0.40		1.5E-03	77
	CA311	4	ridge/ slough		1/15/03	2.0E-05	0.385	0.28	0.5	0.45	31	0.41	0.45		1.7E-03	87
	CA311	4	ridge/ slough		3/15/03	2.0E-05	0.2	0.09	0	0.2	31	0.41	0.20		4.0E-04	20
	CA311	4	ridge/ slough		1/15/03	2.0E-05	0.55	0.44	0.3	0.25	31	0.41	0.25		1.4E-03	69
	CA311	4	ridge/ slough		3/15/04	2.0E-05	0.2	0.09	0.35	0.15	31	0.41	0.15		3.0E-04	15

	CA31 1	4	ridge/ slough		11/15/04	2.0E-05	0.65	0.54	0.3	0.5	31	0.41	0.50		3.3E-03	163
ENP	GL	5	ridge/ slough		12/15/03	5.4E-05	0.63	0.49	N/A	N/A	32	0.65	1.6		1.0E-02	187
	GL	5	ridge/ slough		3/15/04	5.2E-05	0.21	0.07	N/A	N/A	32	0.65	0.6		1.3E-03	24
	GL	5	ridge/ slough		8/15/05	5.4E-05	0.78	0.64	N/A	N/A	32	0.65	1.55		1.2E-02	224
	GL	5	ridge/ slough		6/15/06	4.9E-05	0.32	0.18	N/A	N/A	32	0.65	0.15		4.8E-04	10

References:

1. Harvey, J. W., Schaffranek, R. W.,Noe, G. B., Larsen, L. G., Nowacki, D. J., and O'Connor, B. L. (2009), Hydroecological factors governing surface water flow on a low-gradient floodplain, Water Resour. Res., 45, W03421, doi:10.1029/2008WR007129.
2. Harvey, J.W., Choi, J., Larsen, L., Skalak, K., Psaltakis, J.W., Buskirk, B.A., Swartz, A.G., Lewis, J.M., Gomez-Velez, J.D., Maglio, M.M., Langstrom, T., and Walker, A. (2018), High-Flow Field Experiments to Inform Everglades Restoration: Experimental Data 2010 to 2018: U.S. Geological Survey data release, doi.org/10.5066/P9T2624X.
3. Schaffranek, R. W. and Riscassi, A. L. (2005), Flow Velocity, Water Temperature, and Conductivity at Selected Locations in Shark River Slough, Everglades National Park, Florida; July 1999 - July 2003, doi.org/10.3133/ds110
4. Min, J. H., Paudel, R., Jawitz,J. W. (2010), Spatially distributed modeling of surface water flow dynamics in the Everglades ridge and slough landscape, Journal of Hydrology 390, 1-12, doi:10.1016/j.jhydrol.2010.06.023
5. He, G., Engel, V., Leonard, L. A., Croft, A., Childers, D., Laas, M., Deng, Y., Solo-Gabriele, H. M. (2010), Factors Controlling Surface Water Flow in a Low-gradient Subtropical Wetland, Wetlands, 30, doi:10.1007/s13157-010-0022-1

G. Acknowledgements

This report was prepared in cooperation with the South Florida Water Management District as a part of the USGS-SFWMD cooperative agreement 20HWCOLL0003. It has been peer reviewed and approved for release by the U.S. Geological Survey. We thank Laurel Larsen for assistance with data analysis and Jah Sah at Florida International University for providing the RECOVER microtopography and vegetation mapping data set. We also greatly appreciate the peer reviews provided by Wasantha Lal and Clay Brown of the South Florida Water Management District. Any use of trade, firm, or product names is for descriptive purposes only and does not imply endorsement by the U.S. Government.

H. References

Carter, V., Reel, J.T., Rybicki, N.B., H. A. Ruhl, Gammon, P.T., Lee, J.K. (1999a), Vegetative resistance to flow in south Florida; summary of vegetation sampling at sites NESRS3 and P33, Shark River slough, November 1996. OFR 99-218.

Carter, V., Ruhl, H.A., Rybicki, N.B., Reel, J.T., Gammon, P.T. (1999b), Vegetative resistance to flow in South Florida; summary of vegetation sampling at sites NESRS3 and P33, Shark River slough, April 1996. OFR 99-187.

Casey, S.T., Cohen, M.J., Acharya, S., Kaplan, D.A., Jawitz, J.W. (2016), Hydrologic controls on aperiodic spatial organization of the ridge–slough patterned landscape, Hydrol. Earth Syst. Sci., 20, 2975– 3010, doi:10.5194/hess-20-4457-2016.

Choi, J., Harvey, J.W. (2013), Relative Significance of Microtopography and Vegetation as Controls on Surface Water Flow on a Low-Gradient Floodplain, Wetlands, 34, 101-115, DOI 10.1007/s13157-013-0489-7.

Choi J., Harvey J.W. (2016) Predicting outcomes of restored Everglades high flow: a model system for scientifically managed floodplains. Restoration Ecology. https://doi.org/10.1111/rec.12479.

Harvey, J.W., Choi, J. (2022), Biophysical Data for Simulating Overland Flow in the Everglades, U.S. Geological Survey data release, https://doi:10.5066/P9DQYB1O.

Harvey, J.W., Choi, J., Larsen, L., Skalak, K., Psaltakis, J.W., Buskirk, B.A., Swartz, A.G., Lewis, J.M., Gomez-Velez, J.D., Maglio, M.M., Langstrom, T., Walker, A. (2018), High-Flow Field Experiments to Inform Everglades Restoration: Experimental Data 2010 to 2018: U.S. Geological Survey data release, https://doi.org/10.5066/P9T2624X.

Harvey, J. W., Wetzel, P.R., Lodge, T.E., Engel, V.C., Ross, M.S. (2017), Role of a naturally varying flow regime in Everglades restoration. Restoration Ecology. https://doi.org/10.1111/rec.12558.

Harvey, J. W., Saiers, J.E., Newlin, J.T. (2005), Solute transport and storage mechanisms in wetlands of the Everglades, south Florida, Water Resour. Res., 41, W05009, doi:10.1029/2004WR003507.

Harvey, J. W., Schaffranek, R.W., Noe, G.B., Larsen, L.G., Nowacki, D.J., O'Connor, B.L. (2009), Hydroecological factors governing surface water flow on a low-gradient floodplain, Water Resour. Res., 45, W03421, doi:10.1029/2008WR007129.

Harvey, J. W., Noe, G.B., Larsen, L.G., Nowacki, D.J., McPhillips, L.E. (2011), Field flume reveals aquatic vegetation's role in sediment and particulate phosphorus transport in a shallow aquatic ecosystem, Geomorphology, 126, 297–313, doi:10.1016/j.geomorph.2010.03.028.

He, G., Engel, V., Leonard, L., Croft, A., Childers, D., Laas, M., Deng, Y., Solo-Gabriele, H.M. (2010), Factors controlling surface water flow in a low-gradient subtropical wetland. Wetlands 30:275–286, https://doi.org/10.1007/s13157-010-0022-1.

Jones, J.W., Desmond, G. B., Henkle, C., Glover, R. (2012), An approach to regional wetland digital elevation model development using a differential global positioning system and a custom-built helicopter-based surveying system, International Journal of Remote Sensing, 33:2, 450-465, DOI: 10.1080/01431161.2010.533212.

Kadlec, R. H. and Knight, R. L. (1996), Treatment Wetlands, Lewis Publishers, Boca Raton, 893 p.

Kaplan, D.A., Paudel, R., Cohen, M.J., Jawitz, J.W. (2012), Orientation matters: Patch anisotropy controls discharge competence and hydroperiod in a patterned peatland. Geophysical Research Letters, 39, L17401. https://doi.org/10.1029/2012GL052754.

Lal, A. M. W., M. Z. Moustafa, and W. M. Wilcox (2015), The use of discharge perturbations to understand in situ vegetation resistance in wetlands, Water Resour. Res., 51, 2477–2497, doi:10.1002/2014WR015472.

Lal, A.W. (2020). Analytical Methods and Field Applications to Test the TVDLF Method in Hillslopes and Wetlands, J. Hydraulic Engineering, Vol. 147, DOI: 10.1061/(ASCE) HY.1943-7900.0001819.

Larsen, L.G., Harvey, J.W., Crimaldi, J.P. (2009), Predicting bed shear stress and its role in sediment dynamics and restoration potential of the Everglades and other vegetated flow systems. Ecological Engineering, 35(12), 1773–1785.

Larsen, L.G., Harvey, J.W. (2011), Modeling of hydroecological feedbacks predicts distinct classes of landscape pattern, process, and restoration potential in shallow aquatic ecosystems, Geomorphology, 126, 279-296, doi:10.1016/j.geomorph.2010.03.015

Larsen, L.G., Choi, J., Nungesser, M.K., Harvey, J.W. (2012), Directional connectivity in hydrology and ecology. Ecological Applications, 22(8), 2204–2220.

Larsen, L.G., Ma, J., Kaplan, D. (2017), How important is connectivity for surface water fluxes? A generalized expression for flow through heterogeneous landscapes. Geophysical Research Letters, 44, 10,349–10,358, https://doi. org/10.1002/2017GL075432.

Li, J., Du, Q. and C. Sun (2009) An improved box-counting method for image fractal dimension estimation, Pattern Recognition Vol 42, 2460-2469, doi:10.1016/j.patcog.2009.03.001.

McVoy, C.W., Said, W.P., Obeysekera, J., VanArman, J.A., Dreschel, T.W. (2011), Landscapes and Hydrology of the Predrainage Everglades. Gainesville, FL: University Press of Florida.

Min, J. H., Paudel, R., Jawitz, J.W. (2010), Spatially distributed modeling of surface water flow dynamics in the Everglades ridge and slough landscape, Journal of Hydrology Vol 390, 1-12, DOI:10.1016/j.jhydrol.2010.06.023

Nepf, H. M. (1999), Drag, turbulence, and diffusion in flow through emergent vegetation, Water Resour. Res., 35(2), 479 – 489, doi:10.1029/1998WR900069.

Nungesser, M.K. (2011), Reading the landscape: temporal and spatial changes in a patterned peatland, Wetlands Ecol Manage, 19:475-493, DOI 10.1007/s11273-011-9229-z.

Ross, M.S., Heffernan, J. B., Sah, J. P., Isherwood, E., Blanco, J. (2015), Landscape Pattern- Ridge, Slough, and Tree Island Mosaics. Annual Report submitted to US Army Engineer Research and Development Center. Cooperative Agreement #: W912HZ-10-2-0030. Year 5 Report (2010-2015): 95 pp.

Ross, M.S., Reed, D.L., Sah, J.P., Ruiz, P.L., Lewin, M.T. (2003), Vegetation: environment relationships and water management in Shark Slough, Everglades National Park. Wetlands Ecology and Management **11**: 291-303.

Ronayne, M.J., Gorelick, S.M. (2006), Effective permeability of porous media containing branching channel networks. Physical Review E. http:dx.doi.org/10.1103/ PhysRevE.73.026305.

Rutchey, K., Schall, T.N., Doren, R.F., Atkinson, A., Ross, M.S., D.T. Jones, M. Madden, L. Vilchek, K.A. Bradley, J.R. Snyder, J.N. Burch, T. Pernas, B. Witcher, M. Pyne, R. White, T.J. Smith, J. Sadle, C.S. Smith, M.E., Patterson, G. (2006), Classification for South Florida Natural Areas. U.S. Geological Survey, Open File Report 2006-1240, St. Petersburg, FL.

Rutchey, K., Schall, T., Sklar, F. (2008), Development of vegetation maps for assessing everglades restoration progress. Wetlands, 28(3) pp.806-816.

Rybicki, N. B., Reel, J.T., Ruhl, H.A., Gammon, P.T., Carter, V. (2001), Vegetative resistance to flow in South Florida; summary of vegetation sampling in Taylor Slough, Everglades National Park, September 1997-July 1998. OFR 2001-102.

Rybicki, N.B., Reel, J.T., Gammon, P.T., Garrett, M.K. (2002), Vegetative Resistance to Flow in South Florida Everglades: Summary of Vegetation Sampling in Water Conservation Area 2A, September 1999. OFR 2002-38.

Said, W.P., Brown, M.C. (2013), Hydrologic Simulation of the Predrainage Greater Everglades Using the Natural System Regional Simulation Model v3.5.2, South Florida Water Management District, Water Resources Division.

Schaffranek, R.W., Riscassi, A.L. (2005), Flow Velocity, Water Temperature, and Conductivity at Selected Locations in Shark River Slough, Everglades National Park, Florida; July 1999 - July 2003, doi.org/10.3133/ds110

Schutten, J., Davy, A.J. (2000), Predicting the hydraulic forces on submerged macrophytes from current velocity, biomass and morphology. Oecologia 123, 445–452.

Vogel, S., (1994), Life in Moving Fluids: The Physical Biology of Flow. Princeton University Press, Princeton, NJ, 486 pp.

Yuan, J., Cohen, M., (2017), Spatial metrics for detecting ecosystem degradation in the ridge-slough patterned landscape. Ecological Indicators 74: 427-440, http://dx.doi.org/10.1016/j.ecolind.2016.12.015

Appendix A: Twenty-three subsetted areas from selected vegetation maps binarized to distinguish Ridge (red) and Slough (blue) areas for landscape pattern analysis

WCA-3A North

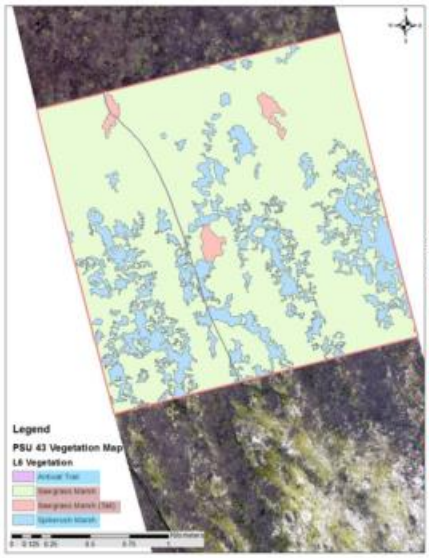

Θ=14.4˚, WxH=1930.5mx1943m, R=970m

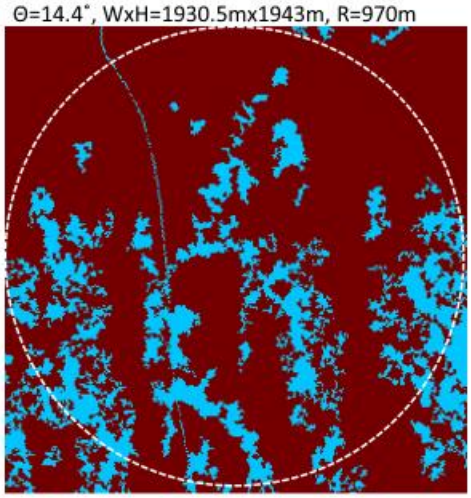

PSU-43_binary.txt

WCA-3A North

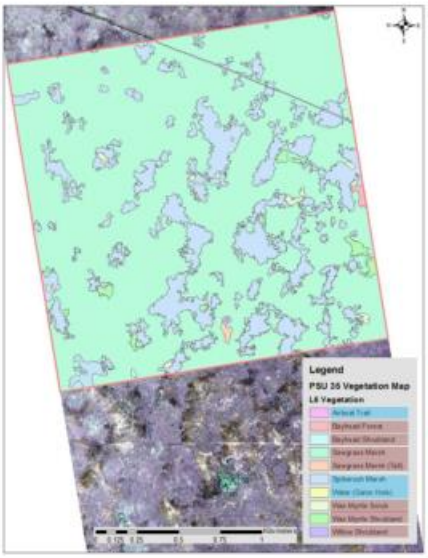

Θ=9.0˚, WxH=1943.5mx1976m, R=971m

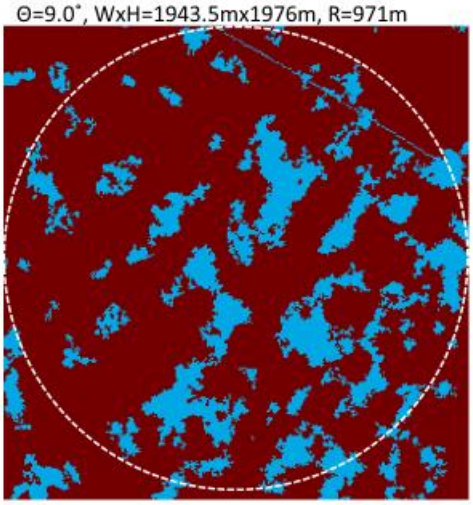

PSU-35_binary.txt

WCA-3A Central East

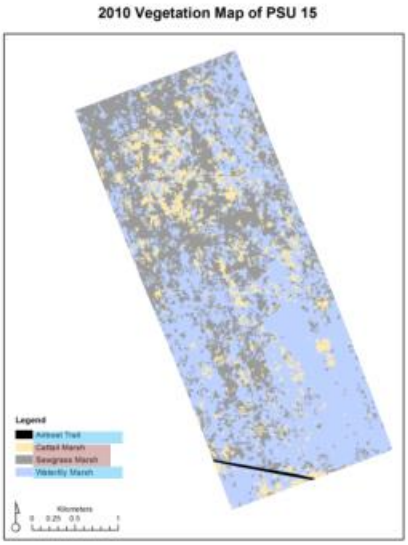

Θ=21.8˚,
WxH=1924mx4927m,
R=962m

PSU-15_binary-1.txt

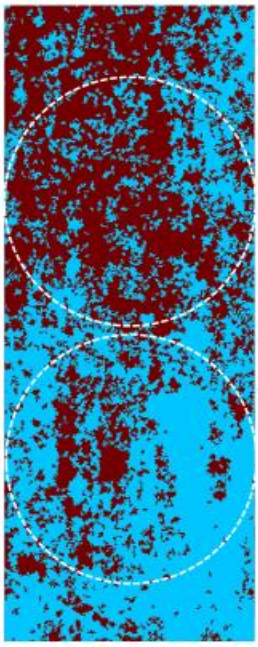

PSU-15_binary-2.txt

WCA-3A Central East

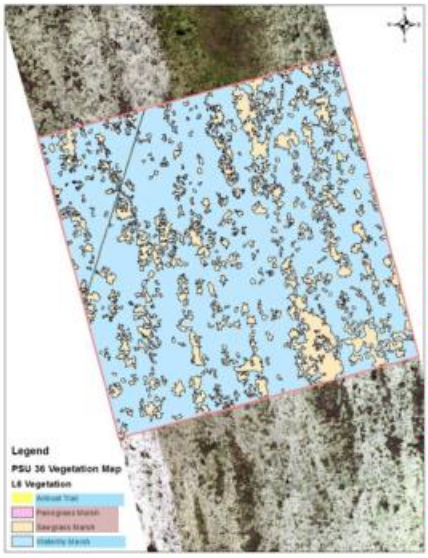

Θ=15.5˚, WxH=1963mx1969m, R=981m

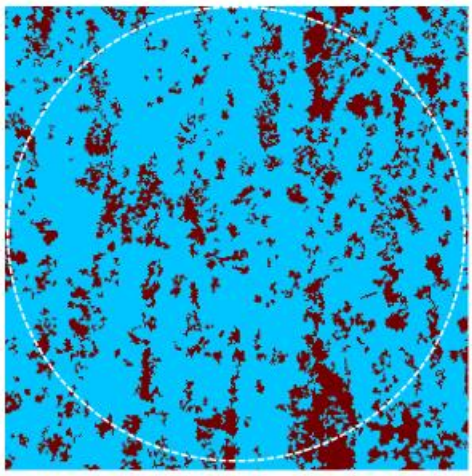

PSU-36_binary.txt

WCA-3A Central East

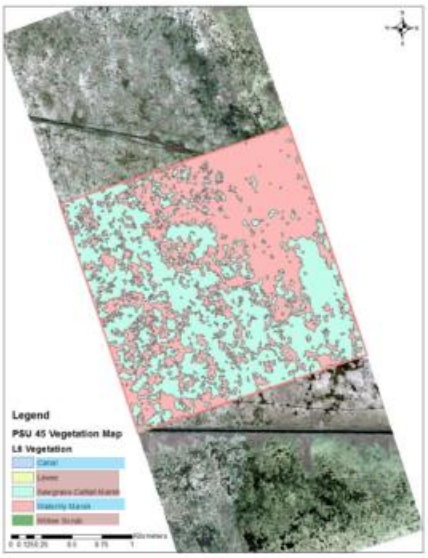

Θ=18.8˚, WxH=1969mx1969m, R=984m

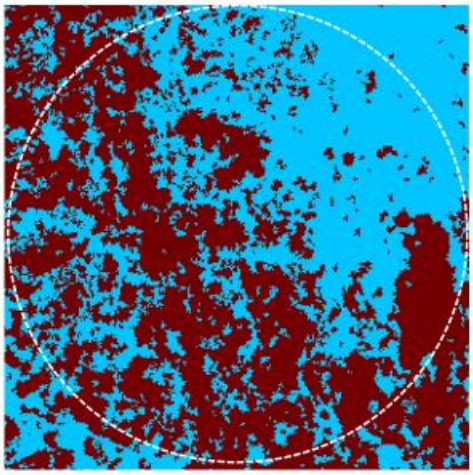

PSU-45_binary.txt

WCA-3A Central West

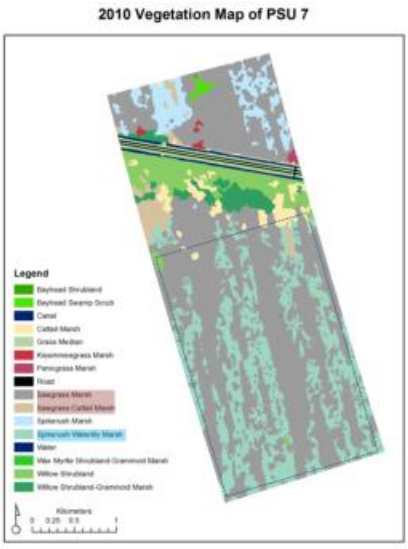

Θ=14.8˚, WxH=1859mx2925m, R=929m

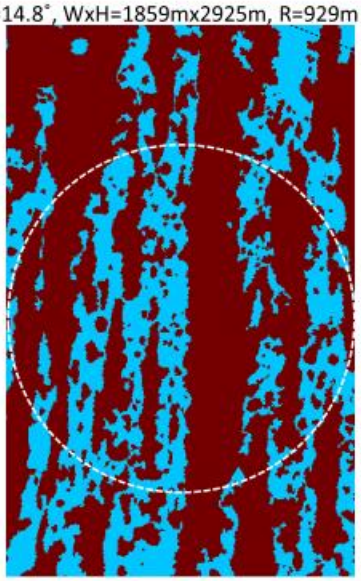

PSU-7_binary.txt

WCA-3A Central West

2010 Vegetation Map of PSU 23

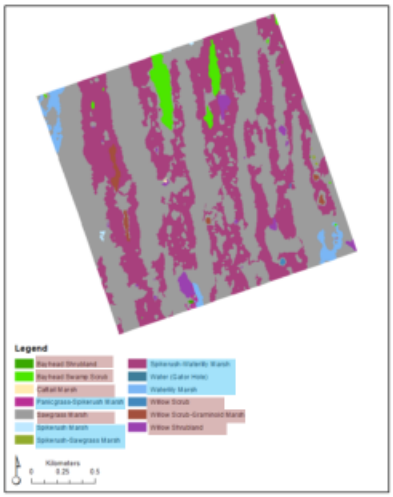

Θ=19.4˚, WxH=1943.5mx1963m, R=971m

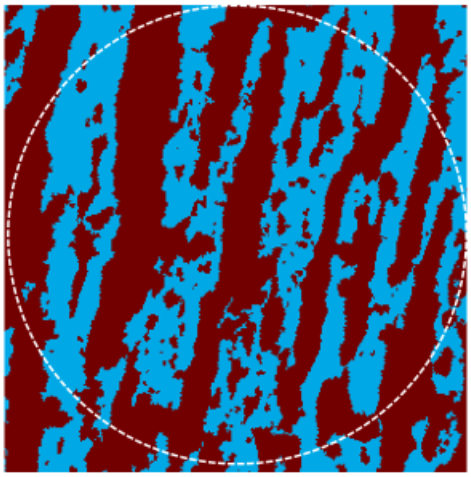

PSU-23_binary.txt

WCA-3A Central West

2010 Vegetation Map of PSU 31

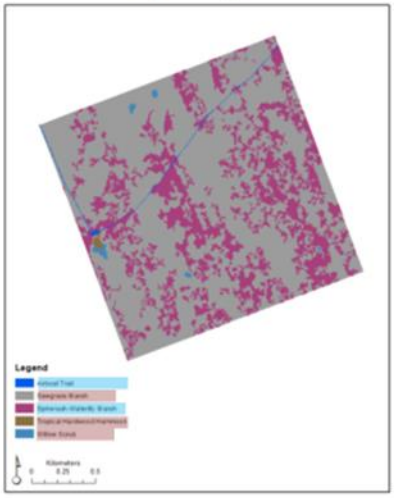

Θ=20.6˚, WxH=1911mx1917m, R=955m

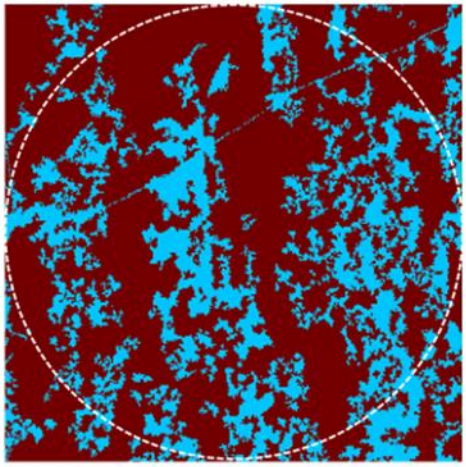

PSU-31_binary.txt

WCA-3A Central West

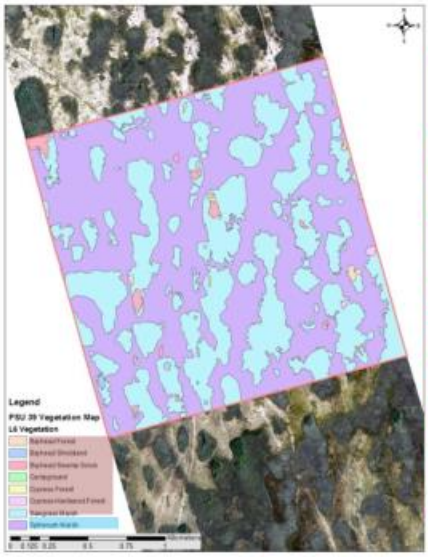

Θ=15.6˚, WxH=1969mx1982m, R=984m

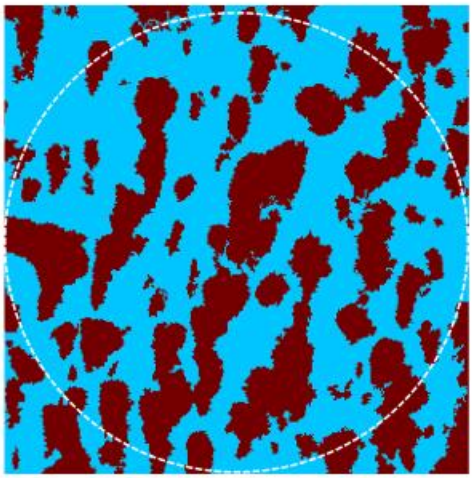

PSU-39_binary.txt

WCA-3A South

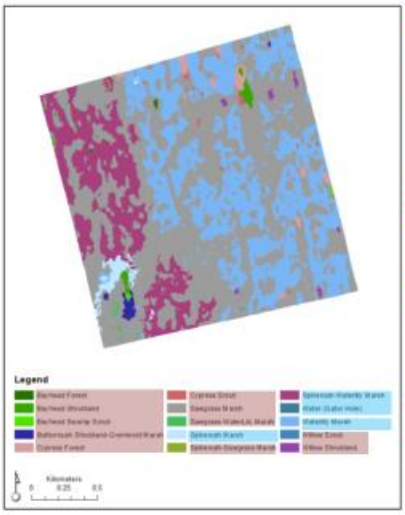

Θ=14.65˚, WxH=1956mx1982m, R=978m

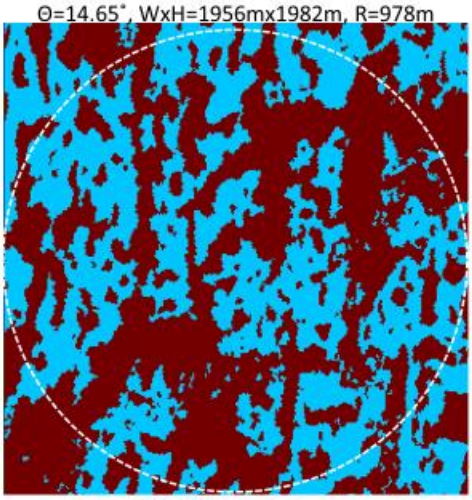

PSU-26_binary.txt

WCA-3A South

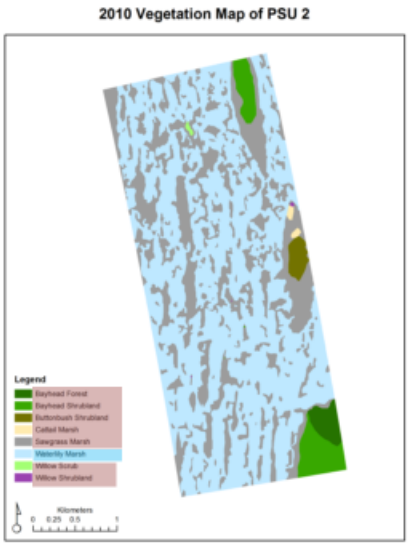

Θ=11.7˚,
WxH=1891mx4933m
, R=945m

PSU-2_binary-1.txt

PSU-2_binary-2.txt

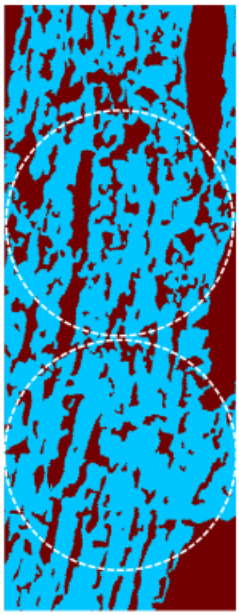

WCA-3A South

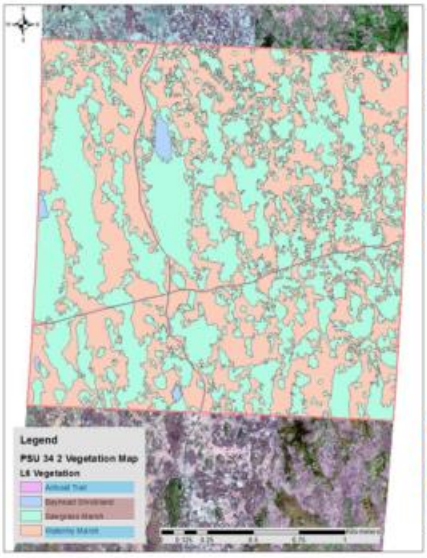

Θ=-1.75˚, WxH=1956mx1956m, R=978m

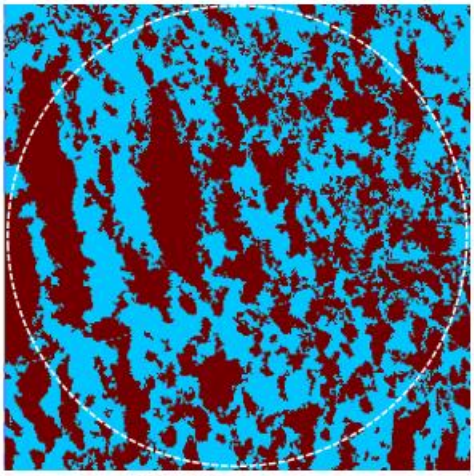

PSU-34_binary.txt

WCA-3B

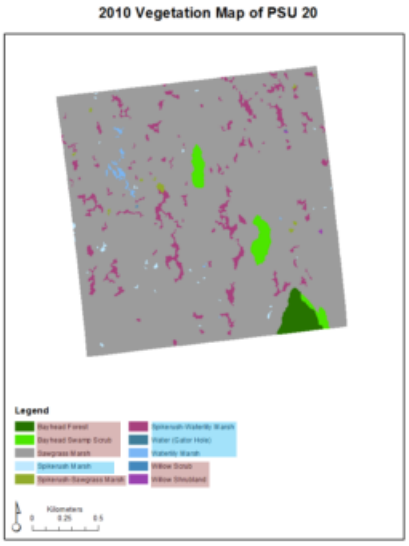

Θ=7.49˚, WxH=1423mx1430m, R=711m

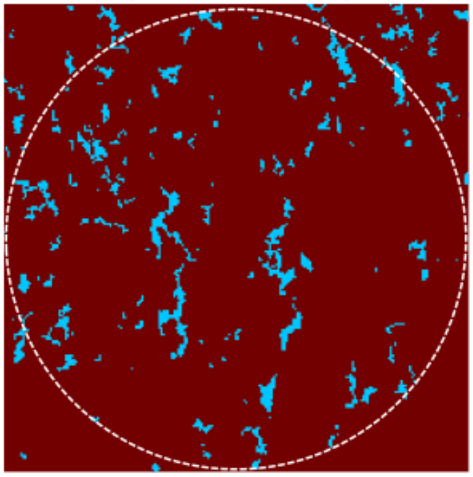

PSU-20_binary.txt

WCA-3B

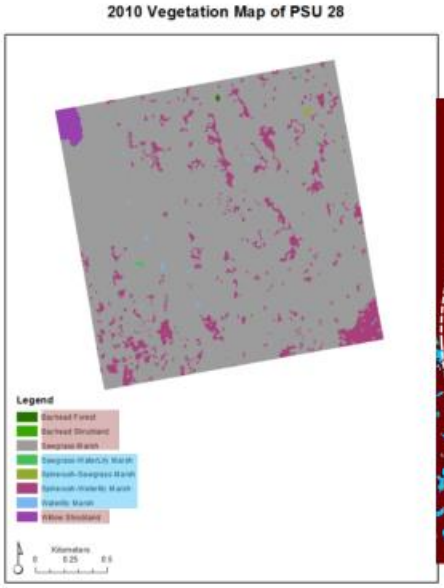

Θ=9.95˚, WxH=1969mx1969m, R=984m

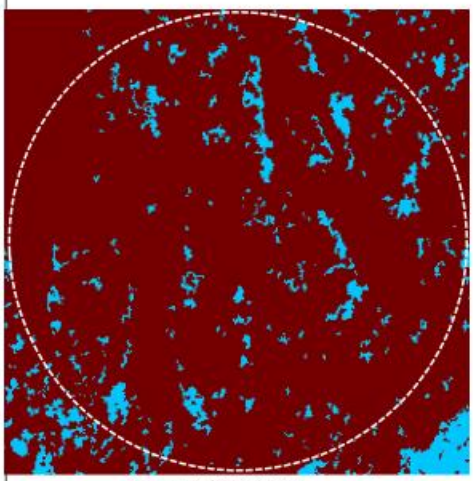

PSU-28_binary.txt

WCA-3B

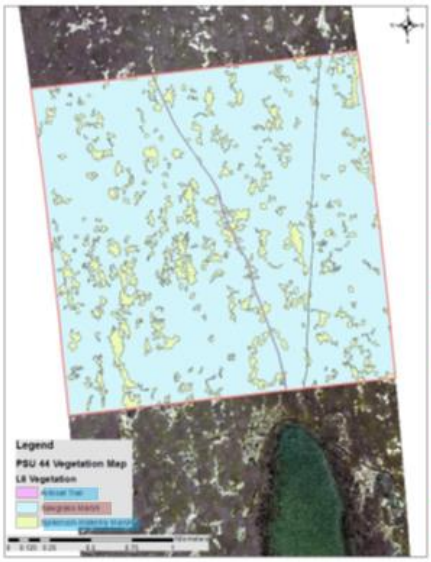

Θ=6.73˚, WxH=1963mx1969m, R=981m

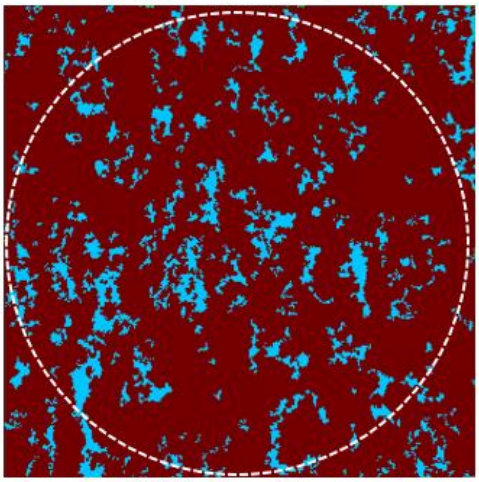

PSU-44_binary.txt

WCA-3B

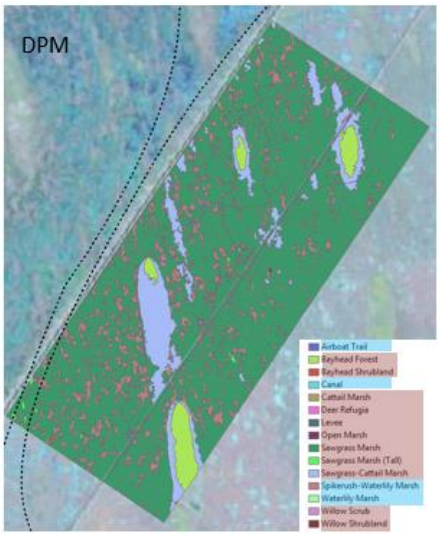

Θ= -34.4˚,
WxH=2873mx7364m,
R=915m

DPM_binary-1.txt

DPM_binary-1.txt

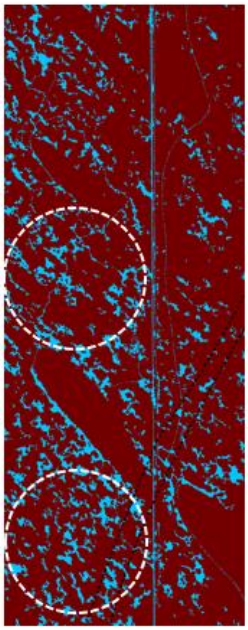

ENP

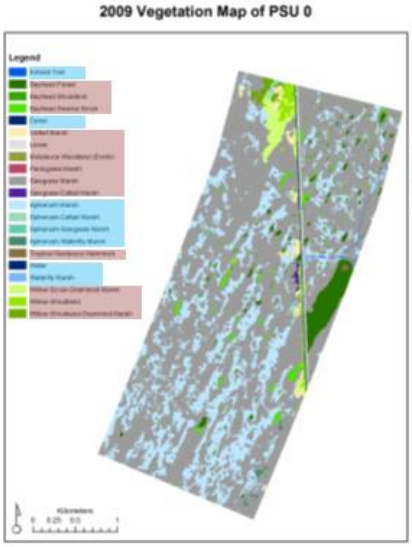

Θ= -20.99˚,
WxH=1859mx4810m,
R=929m

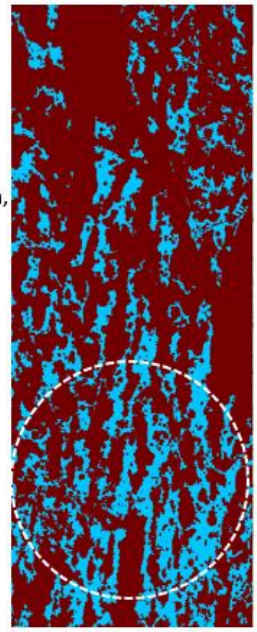

PSU-0_binary.txt

ENP

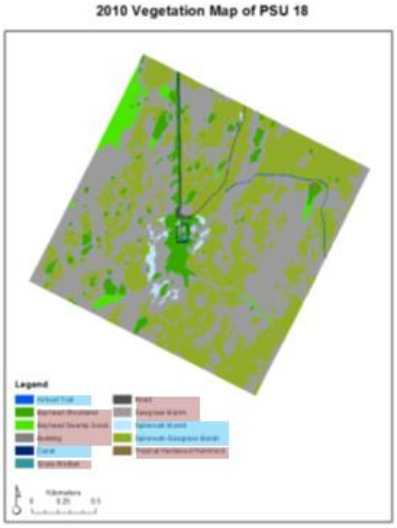

Θ= -25.8˚, WxH=1943mx1950m, R=971m

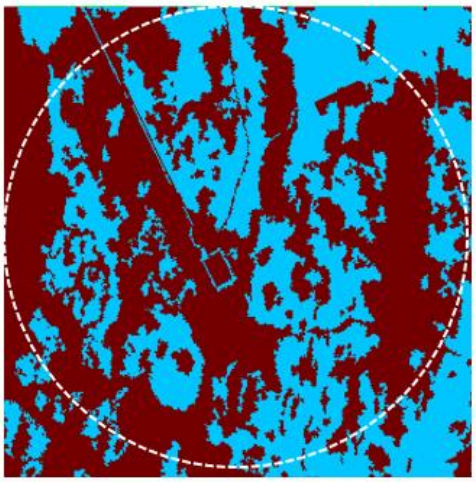

PSU-18_binary.txt

ENP

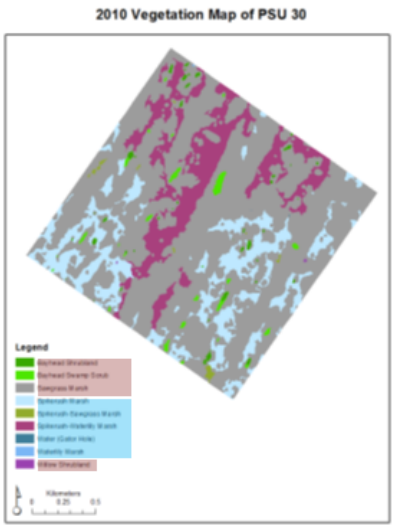

Θ= -34.66˚, WxH=1956mx1976m, R=978m

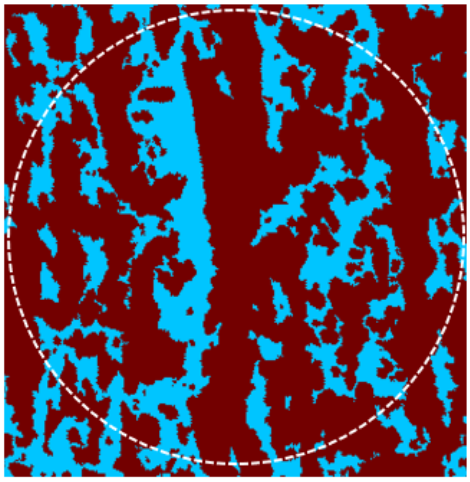

PSU-30_binary.txt

ENP

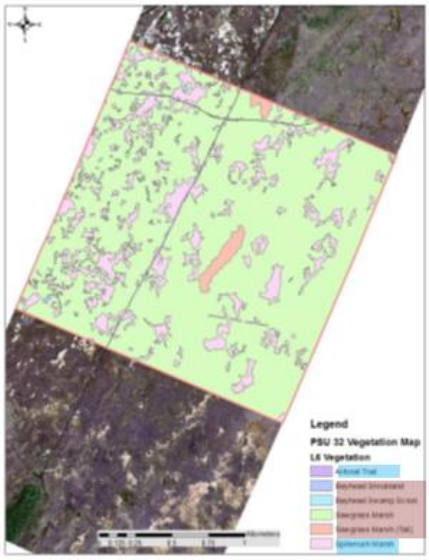

Θ= -22.96˚, WxH=1969mx1976m, R=984m

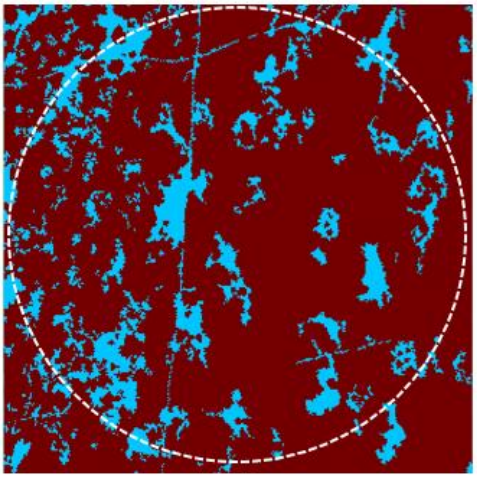

PSU-32_binary.txt